A Final Technical Report

submitted to
U.S. Department of Energy
Office of Energy Efficiency and Renewable Energy

Federal Grant Number: DE-EE0008232

Title: Boosting Energy Efficiency of Heterogeneous Connected Automated Vehicle (CAV) Fleets via Anticipative and Cooperative Vehicle Guidance

Principal Investigator: Ardalan Vahidi, Professor of Mechanical Engineering
208 Fluor Daniel Building, Clemson University,
Clemson, SC 29634
avahidi@g.clemson.edu, (864) 656-4718

Submitting Official: Ardalan Vahidi

Submission Date: December 2, 2020

DUNS Number: 042629816

Recipient Organization: Clemson University
230 Kappa St., Suite 200, Clemson, SC 29634

Project Period: 09-01-2017 to 04-30-2020

Report Number: DOE-Clemson- EE0008232

Executive Summary

In 2017, the Department of Energy funded a team at Clemson University and Argonne National Laboratory to develop collaborative perception and anticipative/predictive vehicle guidance schemes for Connected and Automated Vehicles (CAVs) and to quantify the energy saving potential of this technology in large scale traffic microsimulations at different levels of technology penetration and also experimentally. The project goal was demonstrating up to a 10% energy saving potential from different aspects of the implementation with a focus on reducing unnecessary braking events by anticipatory speed and lane selection. A high-level overview of the project is shown below:

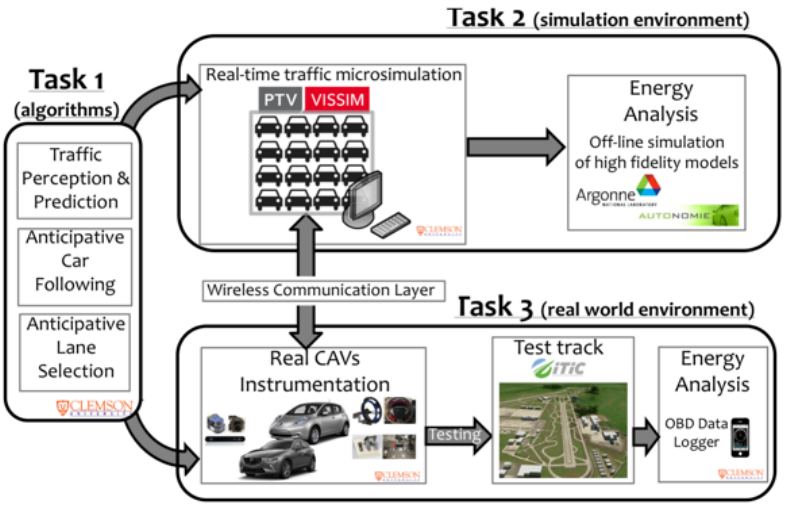

The team has developed novel optimization-based control algorithms for more efficient car-following and lane selection. The algorithms run robustly in a commercial traffic microsimulation environment and also in two instrumented CAVs on a test track, one fully electric and one with a gasoline engine. The vehicles are modified to drive autonomously on a test track and communicate wirelessly to other simulated vehicles and roadside units.

The team has developed and run large scale traffic microsimulations in PTV VISSIM where custom programmed CAVs drive anticipatively to reduce braking and their energy consumption. When following a human driven vehicle, CAVs adjust their distance based on perceived aggressiveness of the preceding vehicle. When following another CAV, they receive the imminent intentions of their preceding vehicles over the next 10-20 seconds via vehicle-to-vehicle connectivity. The energy efficiencies of the fleet for conventional, electric, and hybrid vehicles has been examined in high fidelity simulations. It was found that automated vehicles with gasoline engines perform at a 10% - 20% higher energy efficiency over human drivers. Automated vehicles that are hybrid or fully electric performed at a 3% - 9% higher energy efficiency over human drivers. These results were achieved without compromising traffic compactness. Additionally, due to secondary effects of smoothing traffic flow, energy benefits also apply to human-driven vehicles that

follow automated ones. Such simulated humans were found to drive up to 10% more energy-efficiently than they did in the baseline all-human scenario.

When in addition to car following, lane change maneuvers are optimally decided, the microsimulations show up to 30% energy efficiency benefit at high penetration of CAVs without increasing travel time. Moreover, when two-way collaboration and coordination between CAVs was enabled further efficiency was observed. Impact of communication latency and data loss was also investigated in this project.

Most of the project outcomes have been evaluated experimentally. An important contribution of the project is the proposed Vehicle-in-the-Loop (VIL) testing environment in which experimental CAVs driven on a track interact with surrounding virtual vehicles in real-time. The VIL setup allows the scenarios to be more aggressive because any collision would be with a virtual car that causes no damage or injury.

In the experimental phase, the team explored the energy savings when following city and highway drive cycles, as well as in emergent virtual traffic created from microsimulations. An advanced optimization-based guidance algorithm handles high level velocity planning and benefits from communicated intentions of a preceding CAV or estimated probable motion of a preceding human driven vehicle. A combination of classical feedback control and data-driven nonlinear feedforward control of pedals achieve acceleration tracking at the low level. The controllers are implemented in Robot Operating System (ROS), communication could utilize commercial 4G/5G cellular, and energy is measured via calibrated OBD-II port readings. Up to 8-23% improved energy economy was experimentally recorded over several test days on the test track. The reported improvements are with respect to realistically calibrated human driver car-following and without sacrificing following distance.

This material is based upon work supported by the U.S. Department of Energy's Office of Energy Efficiency and Renewable Energy (EERE) under the Award Number **DE- EE0008232**."

Table of Contents

I. Introduction

This project introduced novel anticipative car following and lane selection schemes for Connected and Automated Vehicles (CAVs). Our control schemes benefited from prediction of human driver behavior, information exchange between CAVs, and sometimes from collaboration to save energy, reduce braking events, and harmonize traffic. The energy savings was first demonstrated by traffic micro-simulations and then via a novel Vehicle-In-the-Loop (VIL) experimental testbed.

II. Accomplishments

a. What are the major goals and objectives of this project?

The main objectives of this project are as follows:

- Incorporate the extended perception schemes that fuse V2X information with those of on-board sensing by each CAV. This is used to construct the current state of surrounding traffic.
- Combine kinematic motion modeling and historical traffic data to create probabilistic prediction models for surrounding vehicles, traffic rules, customs, signals and signs.
- Formulate a vehicle guidance scheme that allows the CAVs to plan their energy optimal and safe future motion plan using the information detailed above.

From the verification point of view, this project follows the approaches listed below:

- To test the effectiveness of the proposed motion prediction scheme, we use high frequency historical and real-time data from Tiger Commute buses.
- To verify the energy efficiency benefit of the proposed vehicle guidance scheme, we use traffic microsimulations.
- To verify the energy efficiency benefit of the proposed vehicle guidance scheme in a near real-world condition, we use test vehicles in a novel vehicle-in-the-loop (VIL) co-simulation environment.

Figure 1 below shows the breakdown of the project into three tasks of: Task 1) Developing Anticipative Vehicle Guidance Algorithms, Task 2) Traffic Microsimulations, and Task 3) Experimental testing via VIL platform. Table I lists the milestones descriptions, and the percentage of completion for each milestone. This Table is populated based on the Statement of Project Objectives (SOPO).

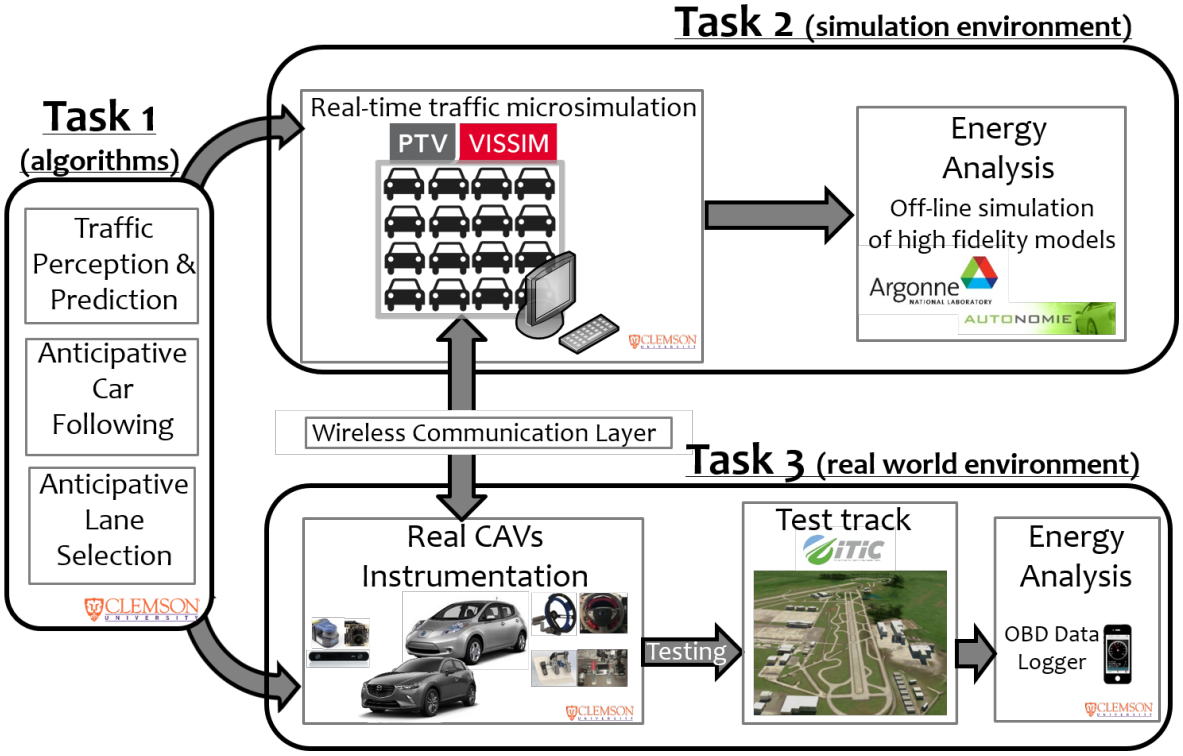

Figure 1: The project breakdown into three tasks.

Table I: The milestones summary based on SOPO and percentage of completion

Milestone	Description	Status
Budget Period 1 (BP-1)		
Milestone 1.1.1 Perception, Estimation and Prediction of Motion of Surrounding Vehicles	Complete integration of algorithms for anticipating longitudinal position and lane of a neighboring vehicle over a 5-10 second future horizon.	100%
Milestone 1.1.2 Perception, Estimation and Prediction of Motion of Surrounding Vehicles	Demonstrate >50% success rate in anticipating the position of a target vehicle within a 10-meter radius of its actual position, 5 seconds in advance	100%
Milestone 2.1.1 Algorithm Design and Custom Code Generation for PTV VISSIM Traffic Microsimulation	Complete coding customized anticipation and predictive guidance functions for the VISSIM microsimulation testbed.	100%

Milestone 2.1.2 Preliminary micro-simulation.	Use simplified energy consumption models to demonstrate >5% average efficiency gain in mixed traffic for CAV penetration >30%.	100%
Milestone 3.1.1 One experimental CAV in Vehicle-in-the-Loop Testbed	Complete vehicle instrumentation, test-track communication setup, and integration with micro simulation environment.	100%
Budget Period 2 (BP-2)		
Milestone 2.2.1 Detailed Energy Consumption Evaluation	Use high-fidelity powertrain models of heterogeneous vehicles to demonstrate >5% (10%) average efficiency gain in mixed traffic for CAV penetration >30% (60%).	100%
Milestone 2.3.1 Collaborative Guidance gain via Traffic Microsimulation	Demonstrate an additional 5% efficiency gain due to collaboration among a group of collaborative CAVs.	100%
Milestone 3.1.2 Experimental vehicle with Anticipative guidance	Demonstrate at least >5% energy efficiency gain for the experimental vehicle as a result of proposed anticipative guidance algorithm.	100%
Milestone 3.2.1 Two experimental CAVs in Vehicle-in-the-Loop Testbed	Demonstrate stable co-simulation of 2 experimental vehicles and <10 virtual vehicles and document >5% average energy efficiency gain for the entire fleet	100%
Milestone 3.3.1 Vehicle-in-the-Loop simulations for multi-lane scenarios	Demonstrate stable co-simulation during lane change operation and document >5% additional average efficiency gain resulting from collaborative driving.	50%*

***** All the low-level control functions are implemented on the car and were tested on the test track. The high-level algorithms are all in mature shape and tested in microsimulations. Only test track verification of lane change remains and is expected to be done over a few days once we are able to test. We had to halt our planned testing after March 7 due to Covid-19 shutdown/considerations. We have completed all other test track testing on car following scenarios as presented in this report. We plan to complete 2 days of testing once we can go back to the test track even though it will be after project close-out.

b. What was accomplished under these goals?

The following subsections describe briefly the accomplishments related to the milestones listed in Table I.

1) Surrounding Vehicle Prediction (Milestones 1.1.1, 1.1.2)

This project requires CAVs to operate in the presence of two types of obstacles. In the first and simpler case, a surrounding vehicle may also be a CAV. Such vehicles can communicate their future intentions, which the ego CAV then uses as preview. On the other hand, mixed traffic will include surrounding vehicles that are not connected. In this case, the ego CAV must predict the surrounding vehicle's motion. This section deals with that prediction task.

A few techniques were developed for predicting surrounding vehicle motion. Data-driven probability models were used as input to earlier car following controllers. To prove real-world feasibility, a Markov model was implemented and evaluated on GPS data from the Tiger Commute bus system. Implementation issues were encountered when adapting the system from MATLAB to C++, leading to the adoption of simpler kinematics-based approaches. A stochastic form of this latter method enabled the chance constraints that are discussed in Section 1-c.

a. Frequentist Probability Models for Car Following

Prediction models for car following focused on the preceding vehicle. CAVs are assumed to use radar and camera sensors capable of detecting the preceding vehicle's (PV's) speed and brake light state. Past measurements were used to form and update a transition matrix containing the probability that a PV will accelerate or brake with a certain intensity at a given future time, given its current speed and brake light state. This algorithm was evaluated in drive cycle simulations where an open-loop vehicle followed the EPA US06 cycle, a second simulated human driver followed that leader, and the CAV predicted that second vehicle's future motion by learning online. The probability model predicted the simulated PV's position within 5 m, 92% of the time, 8 s in advance [6].

b. Predicting Real Bus Motion Using Markov Chains

To evaluate the feasibility of meeting the project's target under real-world conditions, probability models were evaluated using GPS data from the Tiger Commute bus system. In this study, a Markovian probability model was developed that consumed the bus's position, direction, current speed, and change in speed along with time of day to predict the bus's speed over the next step. That speed was then used to compute the bus's future position. Figure 2 shows the model's performance. The dotted lines mark the milestone target of 50% success at predicting position within 10 m. The model was to deliver this performance when predicting up to 10 s, or 2 steps, ahead. Since the 1-step-ahead curve passes above and to the left of the dotted lines' intersection, the milestone target was achieved.

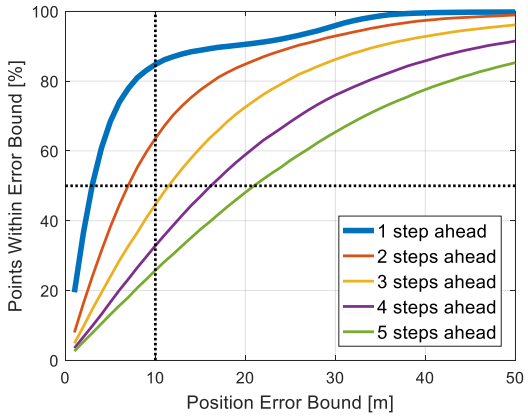

Figure 2: Prediction model performance in the Tiger Commute dataset.

c. Kinematic Techniques Including Probability Distributions

The algorithms in (a) and (b) required higher-dimensional matrices that were not amenable to C++ implementation. Therefore, a simpler approach was desirable for VISSIM and Vehicle-in-the-Loop (VIL) implementation. In car following, constant acceleration was assumed until the vehicle reached either zero or maximum speed. Then, the preceding vehicle was assumed to proceed at constant speed. This prediction technique is stated more formally in [7] and Quarterly Report 10.

A kinematic approach was also applied for lane change algorithms. While constant velocity prediction was used in general, constant acceleration was used for vehicles just downstream of a stopping point and constant braking was used for vehicle just upstream of a stopping point. Laterally, surrounding vehicles were predicted to move with constant speed until they reached the next lane centerline, then proceed along that lane.

If the preceding vehicle's constant acceleration is assumed to be randomly chosen from a distribution, this approach can be used to derive the surrounding vehicle's future position distribution. In this project, the surrounding vehicles' accelerations were assumed normally distributed, resulting in normally distributed positions. By inverting the cumulative distribution function of position, a buffer distance is computed in order to avoid collisions with a specified probability. The inverse cumulative distribution function and specified probabilities are shown in Figure 3, where the linear probability was used in the controller for less conservative performance. Reference [8] (open access) evaluates this chance constraint scheme in a rare, hazardous scenario.

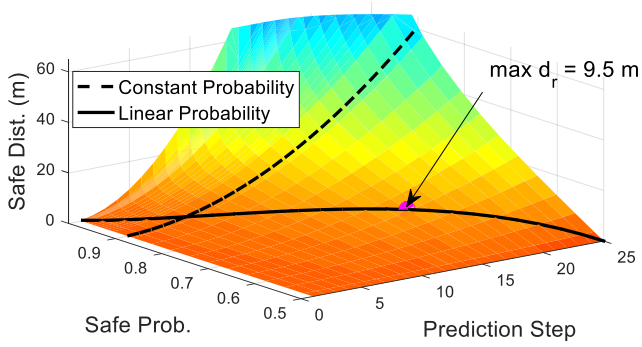

Figure 3: Inverse cumulative distribution function, with constant and linearly decaying safe probabilities overlaid. Figure adapted from [8] (open access)

2) MPC for Car-Following (Milestone 2.1.2)

Section 1 explained that surrounding CAVs can share their future motion plans and that CAVs can predict unconnected surrounding vehicles' future motion. This section will review how such preview was used in car following control. Model predictive control was chosen to take advantage of the control plant's relatively straightforward physics and the availability of preview while accounting for mechanical and safety constraints. This section will briefly describe the car following algorithms and present key simulation results.

a. Base Algorithm

The model predictive controller solves a quadratic program (QP) to find the best sequence of control inputs for minimizing the ego CAV's squared acceleration over a finite prediction horizon of 16 s to 22 s, depending on the type of ego and PV. The commercial solver Gurobi [9] was used to solve the QP, although other commercial and open-source QP solvers are available. Constraints prevent excessive speed, acceleration or braking in excess of mechanical limits, and collisions. A novel application of the Big M method in mathematical programming enabled the controller to operate on heavy diesel trucks with highly non-convex operating spaces. When the PV was unconnected, its trajectory under worst-case braking was used in the constraints to guarantee collision avoidance, although a less conservative approach was adopted later. Reference [6] describes these contributions in greater detail and Quarterly Report 10 provides the convex version of the optimal control problem.

b. MATLAB Simulation Results

Toward Milestone 2.1.2, the MPC car following algorithm was simulated in 8-vehicle strings of closed-loop agents led by one open-loop vehicle that followed the EPA US06 cycle. Vehicles were pseudo-randomly selected to be either connected and automated or unconnected and driven by simulated humans. Their hardware was similarly selected to be either a passenger car or Class 8 truck. 2224 simulation runs were executed to obtain the results shown in Figure 4. Fuel economy was assessed using a Clemson static map-based powertrain model and later verified with Autonomie. Energy results in these early simulations were on track with Milestone 2.1.2, although the benefit was reduced in the presence of heavy vehicles that introduced their own smoothing effect. String space utilization is defined as the average distance from the lead vehicle's front bumper to the trailing vehicle's rear bumper. Conservatism in the worst-case constraints when CAVs followed unconnected vehicles caused the string to lengthen when only a few CAVs were added, but near 100% CAV concentration the strings became shorter than human-like ones. This result guided the later introduction of chance constraints to improve traffic throughput.

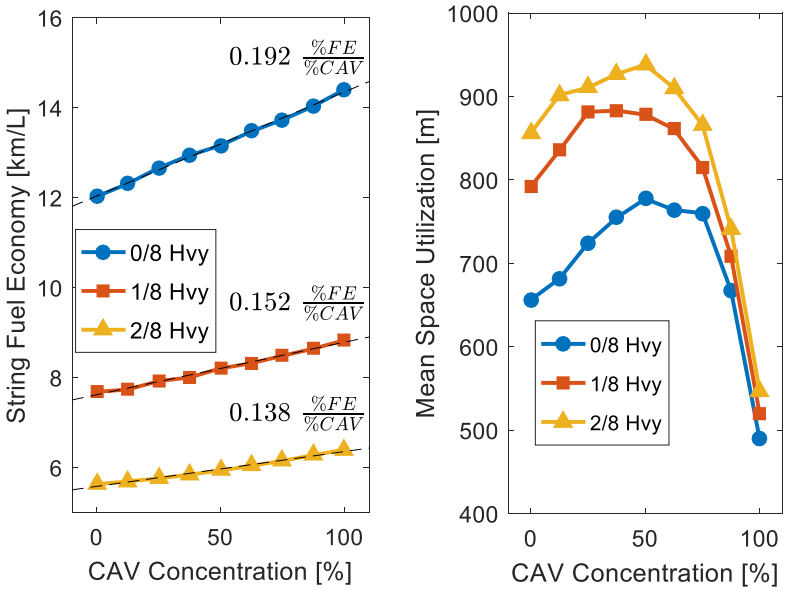

Figure 4: String fuel economy and space utilization in the MATLAB drive cycle simulations. Figure adapted from [6].

3) Mixed Integer Programming Lane Decision Algorithm (Milestone 2.1.2)

In real-world environments, vehicles can sometimes pass one another to avoid disturbances, thereby saving energy. This section will describe the algorithms developed during this project for optimizing future lane change plans jointly with longitudinal acceleration.

a. Base Algorithm

Lane change optimization presents several challenges that were addressed as part of this project. Especially in the presence of human drivers, the automatic controller should feature lane discipline, or the explicit rule of driving inside distinct lanes except during brief lane switching events. It must also tackle the problem of non-convex drivable regions; a CAV can either drive in front of or behind an obstacle, for example. This renders a simple maximum position constraint like the one used in car following insufficient for lane change optimization.

A typical lane change process is linearly approximated such that the time response of lateral position to a step change in lane command is 2nd order. The disjunction of driving upstream or downstream of an in-lane obstacle is handled using the Big M method, and binary indicator variables deactivate collision avoidance constraints when the CAV is outside the obstacle's lane. Reference [8] (open access) provides the multilane model in state-space form along with the position constraints.

Under these constraints, an objective is minimized to promote efficient and timely driving. Laterally, the objective minimizes tracking error relative to a fixed lane reference. The basic 2-lane implementation in [10] also penalized a weighted sum of squared acceleration and squared speed tracking error with a constant speed reference. As in car following, future intentions are shared between CAVs. Figure 5 shows an example trajectory where this controller plans to pass two obstacles.

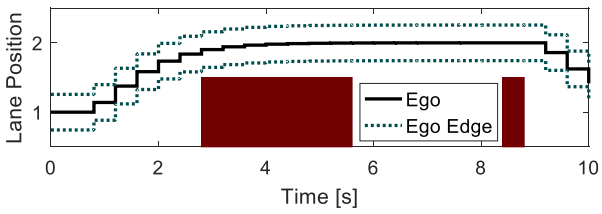

Figure 5: An optimal plan to pass two obstacles, shown in red. Figure adapted from [10].

Early MATLAB simulations in [10] involved a group of 4 CAVs passing a slow-moving obstacle. Compared to a rule-based algorithm that changed lanes in reaction to a slowdown, the anticipative algorithm reduced fuel consumption by 8.4% and travel time by 6.2%. Moreover, this improvement accounted for 80% of *excess* fuel relative to constant-speed operation as shown in Fig. 6.

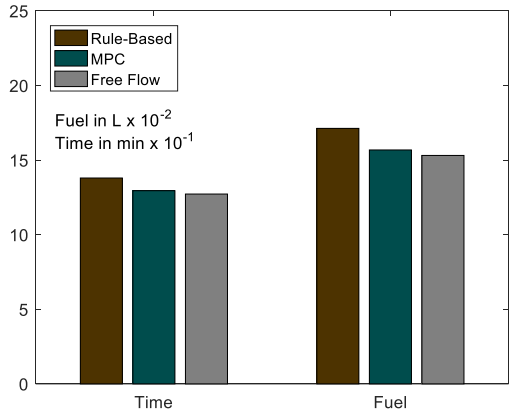

Figure 6: Travel time and fuel consumption performance of the MPC-only multi-lane guidance algorithm. Figure adapted from [10].

b. Hierarchical Architecture

A drawback of the pure-MPC design in Section 3-a is that the longitudinal part of the objective is not optimal for a whole trip or even a whole road link. Together with the expansion to roads with an arbitrary number of lanes, a supervisory planner was added to mitigate MPC's short-sightedness. Using Pontryagin's Minimum Principle, the parabolic velocity trajectory was analytically determined to minimize the square of acceleration over trip. In electric vehicles, it also minimizes cumulative energy consumption [11]. After solving for the parabola's parameters from each step's unique boundary conditions, the resulting state trajectory is passed to the MPC as a reference. The MPC objective is then modified by penalizing deviation from that reference. This hierarchical scheme is documented in detail in [12]. A sample group of MPC solutions are shown in the upper plot of Figure 7, where the lower plot compares the green vehicle's acceleration command to its long-term reference. In this scenario, all vehicles are CAVs and so the surrounding vehicle's future trajectories become constraints.

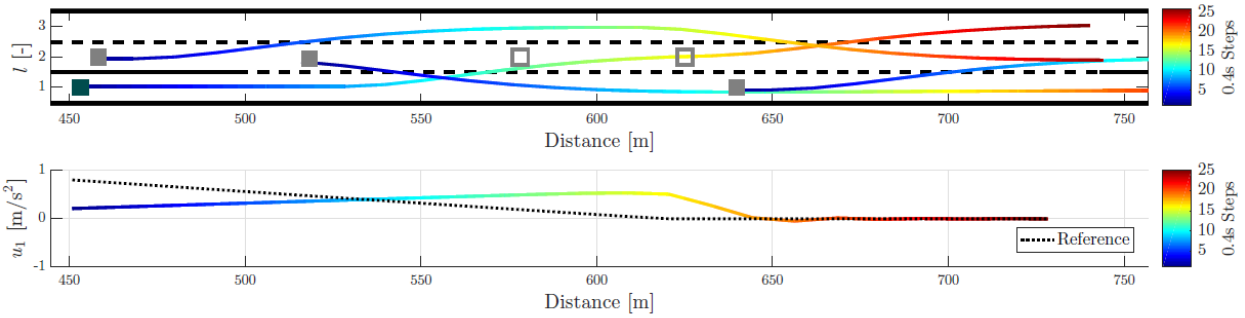

Figure 7: Optimal trajectories of several CAVs in a merging situation (above) and the green CAV's acceleration plan for the same time horizon (below). Figure adapted from [12].

c. Collision Avoidance in Mixed Traffic

In heterogeneous traffic where CAVs interact with unconnected vehicles, surrounding vehicle motion is predicted as described in Section 1-c. The chance constraint design was evaluated in the exceptionally hazardous scenario shown in Figure 8, where the CAV is shown in orange and its following vehicle does not detect it. Several variants of the design were compared in [8] (open access).

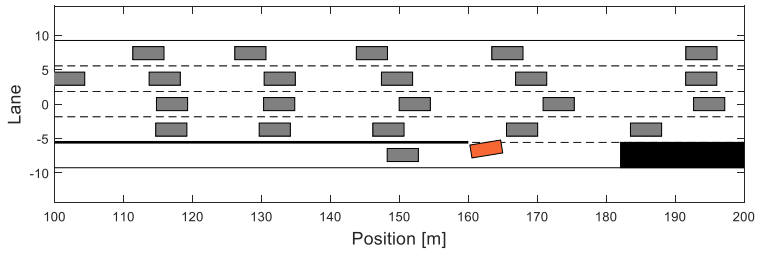

Figure 8: The scenario used to evaluate the chance constraints for unconnected surrounding traffic. The CAV is in orange and unconnected vehicles are in gray.

The chance-constrained controller was further evaluated for energy consumption in an arterial scenario with 12 vehicles. Either 0, 4, 8, or all 12 of them were CAVs and the others were controlled by a combination of a multi-lane rule based lane change algorithm and the Intelligent Driver Model [13]. When travel time was held constant, energy consumption steadily improved as shown in Figure 9 for a 16% benefit at 100% CAV concentration.

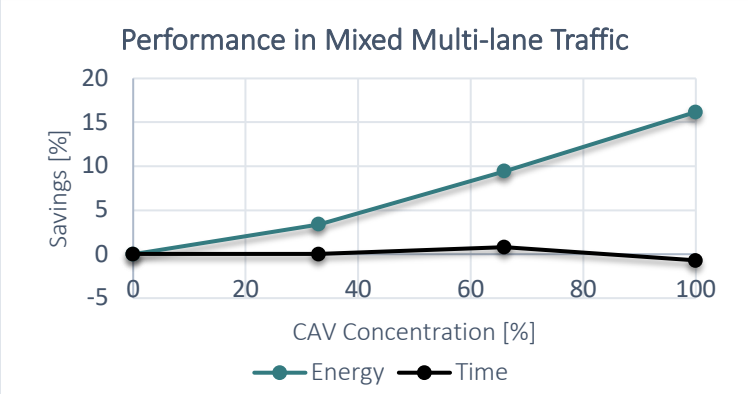

Figure 9: Energy improvements from optimal multi-lane guidance in a mixed traffic, arterial scenario.

4) Improving reliability of connected and automated vehicle (CAV) in urban/sub-urban environments (Milestone 2.1.1)

a. Communication loss in connected vehicles

In urban/suburban vehicular networks, significant radio signal attenuation might occur due to the distance, multipath signal fading, and shadowing, as distance between transmitter and receiver vehicles can vary and signals may move through obstacles, such as buildings, trees, long and tall vehicles (e.g., truck). Communication models that fail to consider realistic road topologies and obstacles may lead to inconsistent results.

For computing the path loss at the receiver, we use the following generalized equation for receive power $P_{Rx}(d)$ at the receiver,

$$P_{Rx}(d) = P_{Tx} + G - \sum PL(d) \qquad (1)$$

where, $P_{Rx}(d)$ is the calculated received power of receiver Rx, for distance d from transmitter Tx; G is the antenna gain. $PL(d)$ contains the path loss components of large-scale path loss and fading, and of deterministic obstacle shadowing, or of stochastic fast fading.

The value of the path loss component $PL(d)$ varies from one path loss model to another. We have studied a number of path loss models for measuring the path loss effect in semi-urban vehicular traffic. We found that different loss models have different impact on the network- and application-level reliabilites. In particular, the Random loss model has the lowest impact, Friis-Nakagami and long distance have the medium impact, and LOS/OLOS/NLOS (Line-of-sight/Obstructed-LOS/Non-LOS) model has the highest impact on the reliability performance. For instance, the network- and application-level reliabilities for LOS/OLOS/NLOS model are 30% and 60% for a moderate Tx-Rx distance. These are not satisfactory for safety-critical applications.

Hence, the research question is how to improve both the network- and application-level reliabilities under a realistic path loss setting. To improve the reliability performance, we propose a feedbackless relaying mechanism which improves the reliability by 35% for LOS/OLOS/NLOS model and by 60% for a number of other studied loss models.

b. Proposed feedbackless relaying technique for improving reliability

For improving the PDR and T-window reliability, we have proposed a relaying mechanism on top of IEEE 802.11p. With the help of a couple of relay vehicles, the overall network performance improves significantly.

In our proposed relaying approach, the selection of a relay vehicle is done autonomously by the system. As there is no acknowledgement packet in DSRC based 802.11p, there is neither an RTS (Request to Send)/CTS (Clear to Send) packet nor an RTB (Request to Broadcast)/CTB (Clear to Broadcast) packet to send. But in our approach, the relay vehicle selection is done by a simple feedbackless yet effective method as discussed below.

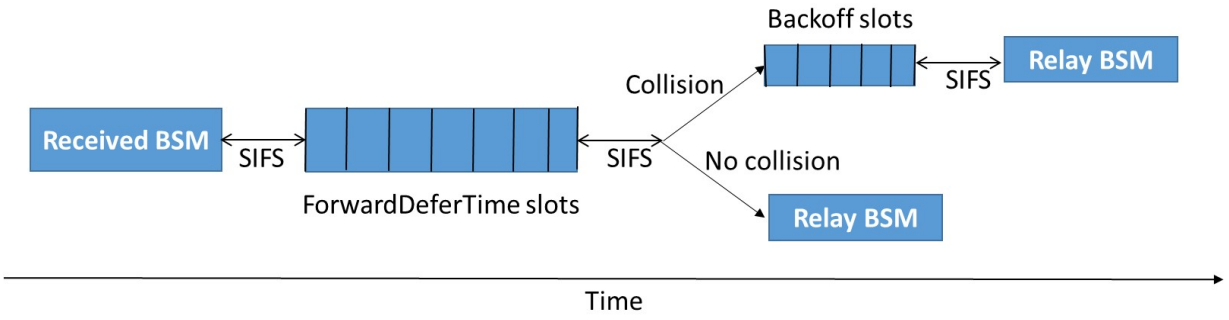

Figure 10: The relaying procedure.

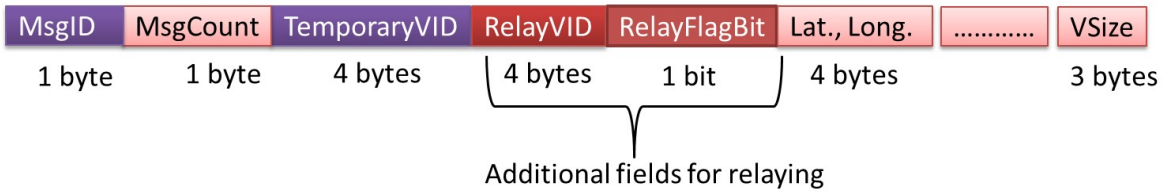

Figure 11: Modified SAE J2735 DSRC BSM frame part I for relaying.

All the connected vehicles are assumed to follow the rules of IEEE 802.11p transmission rules (Carrier Sense Multiple Access with Collision Avoidance (CSMA/CA)). However, for relay vehicle selection, we adopt a simple yet effective intelligent defer mechanism on the top of CSMA/CA. When a vehicle receives a BSM in its direction of motion, it will not forward the BSM immediately; rather, it waits for a *ForwardDeferTime*. *ForwardDeferTime* count down starts following a SIFS (Short Inter-frame Space) and it is done independently by each vehicle. While a sending vehicle V_i sends a packet, the *ForwardDeferTime* of a receiving vehicle V_j inside the communication range R of V_i is computed by,

$$DT_{i,j} = \left\lfloor MaxDeferCount \times \frac{(R-\alpha \times d_{i,j})}{R} \times SlotTime \right\rfloor \quad (2)$$

where $0 < \alpha < 1$ is a tuning parameter to give different defer times to vehicles by giving weight to $d_{i,j}$. We set α at 0.5. $d_{i,j}$ is the Minimum Euclidean Distance between V_i and V_j, which is computed by $d_{i,j} = \sqrt{\left((x_i - x_j)^2 + (y_i - y_j)^2\right)}$, where (x_i, y_i) and (x_j, y_j) are the location coordinates of V_i and V_j, respectively. *MaxDeferCount* is the maximum number of deferred SlotTimes (Typically 20 SlotTimes). A SlotTime is the duration of one slot, which is typically 9 μs. Eq. (2) is computed autonomously by each vehicle. With this computation, the furthest vehicle from the transmitting vehicle will get the shortest defer time, and the closest vehicle will get the longest defer time.

A vehicle V_j, after waiting for $DT_{i,j}$ time, turns around and senses the channel. If it finds the channel is free, it will set the *RelayFlagBit*, add the *RelayVehicleID* on the received BSM packet and rebroadcast after a SIFS time (which is typically 16 μs). On the contrary, if the vehicle finds the channel is busy, which means there is another vehicle further away that is responsible for relaying. Hence, it will discard its $ForwardDeferTime$ and returns to the normal Tx/Rx mode. If a vehicle receives a BSM with *RelayFlagBit* bit set, it will not rebroadcast. In this way, we prevent from rebroadcasting the same packet multiple times.

If a message collision happens (two nodes get the same *ForwardDeferTime*, which is very unlikely), the collision is resolved by a random backoff procedure. The backoff period is chosen randomly from the range of $[0, \frac{DT_{\min}}{2}]$. Note that, in this procedure, only the vehicles whose messages collided will participate. The DT_{min} is computed by,

$$DT_{min} = \left\lfloor MaxDeferCount \times \frac{(R - \alpha \times R)}{R} \times SlotTime \right\rfloor$$

$$DT_{min} = \lfloor MaxDeferCount \times (1 - \alpha) \times SlotTime \rfloor \quad (3)$$

In the backoff stage, if the channel is sensed idle for *SlotTime* time period, the counter is decreased by one. The counter will be frozen if the channel is sensed busy. The counter will be resumed once the channel is sensed idle continuously for a SIFS time period. Finally, the packet will be sent as soon as the counter reaches zero. If the collision cannot be resolved by maximum RET_{max} (< 7) times, the relay node selection is discarded with fallback to the normal periodic 802.11p based broadcast. The relay attempts start again at the next broadcast period. Figure 10 shows the sketch of the above described relaying procedure, and Figure 11 shows the modified SAE J2735 DSRC BSM frame part I for relaying, where two additional fields, *RelayVehicleID* and *RelayFlagBit* are inserted.

For relay node selection in the intersection case, the *ForwardDeferTime* computation (Eq. (2)) will be updated by the following,

$$DT_{i,c} = \left\lfloor MaxDeferCount \times \frac{R}{(R - \alpha \times d_{i,c})} \times SlotTime \right\rfloor \quad (4)$$

where, $d_{i,c}$ is the Minimum Euclidean Distance between vehicle V_i and the intersection-center (c). In Eq. (4), the vehicle closest to the intersection-center will get the minimum defer time and eventually will be selected as a relay node. The collision resolution backoff time (DT_{min} (Eq. 3)) will also be updated accordingly.

c. Simulation setup

An integrated simulator is developed for the traffic and network micro simulation. The vehicular modeling is done using the microscopic traffic simulator PTV VISSIM, and network simulation is performed using ns-3. Table 1 shows the explicit parameters used for VISSIM and ns-3 simulations. Other than the explicit parameters, simulation is conducted under the simulators' default settings.

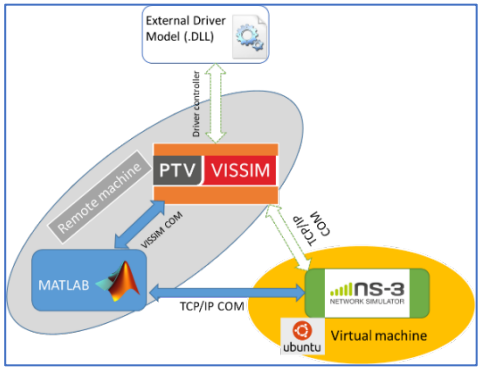

Figure 12: Integrated micro simulator.

Figure 13: VISSIM simulation test network with CU-ICAR neighborhood.

Figure 12 shows the integrated simulator, which consists of PTV VISSIM for traffic simulation, ns-3 for discrete-event network simulation, and MTALAB. MATLAB scripting is used for setting up traffic parameters in VISSIM through VISSIM COM (Component Object Model) and setting real-time communication with ns-3 and VISSIM through TCP/IP socket. The external car following and lane changing could be implemented in external driver model (EDM) through DLL (Dynamic Linked Library).

The VISSIM COM (Component Object Model) interface through MATLAB scripting is used to initiate the desired test track network in VISSIM and send and receive traffic parameters/data in VISSIM-MATLAB interface. Through the TCP/IP socket API (Application Programming Interface) VISSIM is connected with the discrete-event network simulator ns-3 via MATLAB. Every simulation second (each 100 msec), MATLAB sends VISSIM vehicles' position information to ns-3. Ns-3 uses waypoint-mobility-model to create and track the vehicle's position and speed. A number of propagation loss models are used to realize the communication loss among simulated vehicles. Based on the perceived loss, the feedback for suggested car following parameters can be sent to VISSIM through MATLAB, which could be realized by the simulated vehicles in VISSIM. The VISSIM test network is set with 1.3 km stretch CU-ICAR neighborhood traffic road, consisting one roundabout, one car parking, and two intersections. The VISSIM test traffic network is shown in Figure 13.

Table 1. ns-3 simulation settings.

ns-3 Parameter	Value
Number of vehicles	100
BSM size	200 bytes
BSM rate	10 Hz
Frequency	5.9 GHz
Channel Bandwidth	10 MHz
Channel access	802.11p OCB
Data rate	6 Mbps
TXP	23 dB
Encoding	OFDM
Mobility model	Waypoint Mobility (VISSIM vehicle position in every simulation sec)
Receiver sensitivity	-95 dBm
Propagation delay model	Constant Speed Propagation
Propagation loss model	Abstract, Random, Long distance, Friis-Nakagami loss models

d. Performance Analysis

In this section, we study the impact of different loss models on the network-level and application-level performance metrics of connected vehicles in urban/sub-urban area. We study the performance of LOS/OLOS/NLOS loss model as a representative of empirical loss models and the Friis-Nakagami as a representative of joint deterministic and stochastic fading models.

1) Impact on PDR and T-window reliability

Figure 14 exhibits the PDR and the T-window reliability performance under different loss models and no-loss model with different T-window values for varying Tx-Rx communication ranges. As expected, no-loss

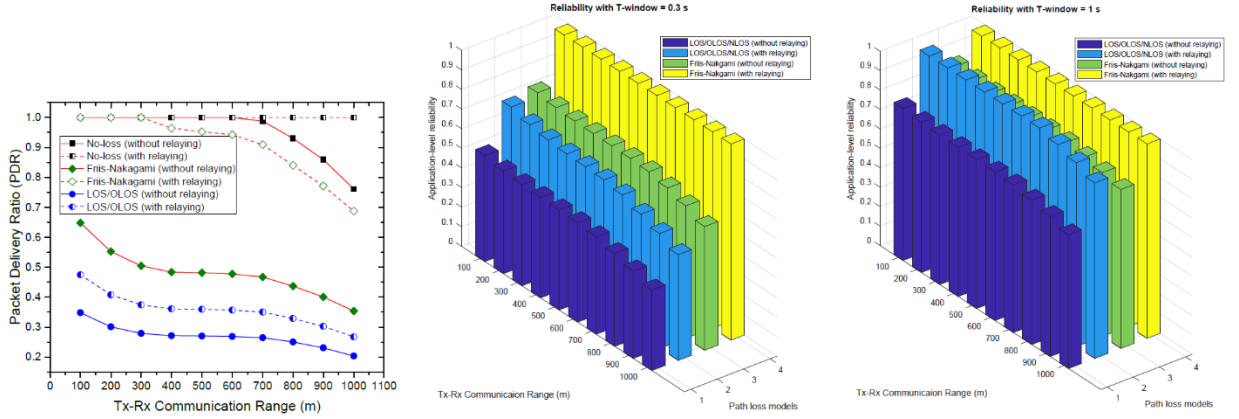

(a) Packet delivery ratio (PDR). (b) Reliability with T-window=0.3 sec. (c) Reliability with T-window=1 sec.

model has the highest PDR and reliability with different values of T-window (Figure 14(a)). PDR only starts dropping from 100% when the Tx-Rx communication distance becomes higher than 600 m. The reliability value depends on the T-window value. A higher T-window value results in a higher reliability. When the Tx-Rx communication range equals 1000 m, the reliabilities of the no-loss model are 85%, 90% and 95% for T-window values equal to respectively, 0.3 sec, 0.5 sec, and 1 sec. However, PDRs and reliabilities are significantly lower with the Friis-Nakgami and LOS/OLOS/NLOS models under the increasing Tx-Rx communication ranges. With the moderate communication distance (300 m), PDRs of Friis-Nakagami and LOS/OLOS/NLOS models are around 50% and 30%, respectively.

Figure 14: PDR and the T-window reliability performance under different loss models.

The Friis-Nakgami model has moderate reliability, which is, over 70% with higher T-window values and around 60% with T-window=0.3 sec. The LOS/OLOS/NLOS model has the lowest reliability. With T-window=1 sec, the reliability range is 70-80%, whereas, for T-window=0.5 sec and T-window=0.3 sec, these ranges are 55-65% and 40-55%, respectively. Hence, with a realistic loss model (such as LOS/OLOS/NLOS), for delay sensitive applications (lower T-window value), reliability is just over 50% for the communication ranges 100-600 m, which is definitely not a satisfactory performance.

Figure 15 shows the PDR and reliability improvement through the proposed relaying technique. Figure

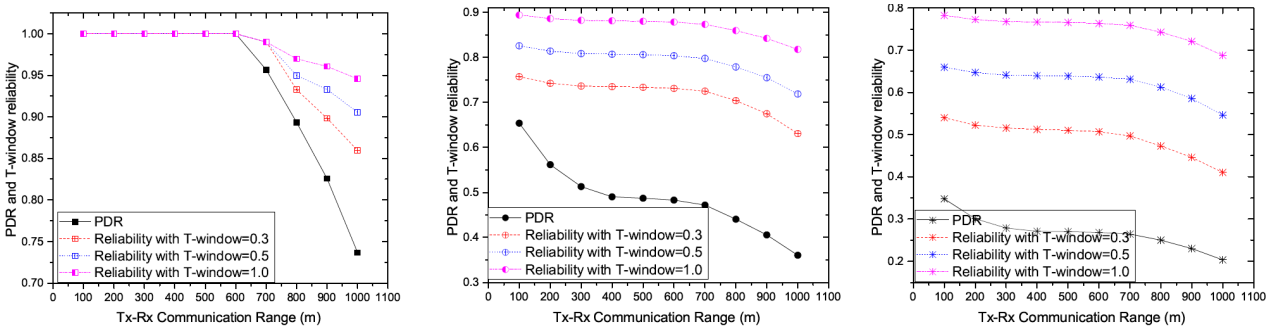

(a) No loss model. (b) Friis-Nakagami loss model. (c) LOS/OLOS/NLOS loss model.

Figure 15: PDR and reliability improvement through relaying.

15(a) shows that with the help of relaying, all the studied loss models improve PDR significantly. Depending on the loss model and the Tx-Rx communication distance, these improvements vary from 30% to over 90%. While with the relaying technique, PDR improvement ranges from 30% to 40% for

LOS/OLOS/NLOS model under different Tx-Rx communication distance, this improvement is over 50%-90% for the Friis-Nakagami model.

For the reliability improvement, Figure 15(b) shows that with T-window equal to 0.3 sec, with the help of relaying, the Friis-Nakagami model achieves almost 100% reliability while the LOS/OLOS/NLOS model achieves around 70% reliability. This improvement is around 35% from their no-relaying reliability value. Nevertheless, with T-window=1 sec, LOS/OLOS/NLOS model also achieves almost 100% reliability even for the Tx-Rx communication distance over 800 m (Figure 15(c)).

2) Impact on latency

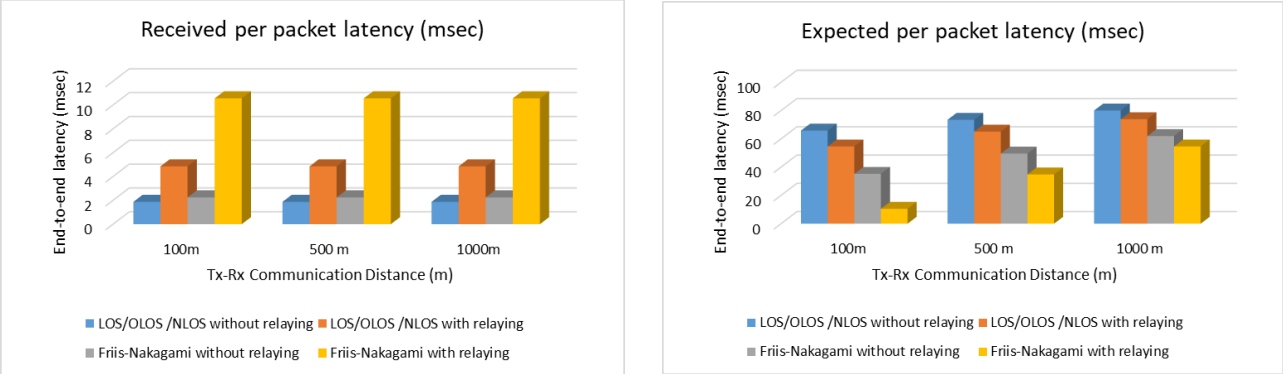

Figure 16: Latency for per received/expected packet. (a) Per received packet latency. (b) Expected per packet latency.

Figure 16 shows the performance in terms of both per received packet and expected per packet latencies. Figure 16(a) shows the per received packet latency with and without relaying. Definitely, relaying increases the latency for both the path loss models. Without relaying, per received packet latency (PRPL) is as low as 2 msec. With relaying, PRPL is at most 10 msec. However, interestingly, with relaying, PRPL of Friis-Nakagami model is higher than that of LOS/OLOS/NLOS model. This is because Friis-Nakagami has more received packets (Figure 15(a)) than LOS/OLOS/NLOS model. Some late arriving received packets may contribute to higher average latency for Friis-Nakagami model, which could be explained considering the other latency metric, expected per packet latency (EPPL) as shown in Figure 16(b). In the EPPL calculation for a fair comparison between the path loss models, both the received packets and dropped packets have been considered. Hence, if a loss model has more dropped packets, it adds to its EPPL latency. Note that each dropped packet adds 100 msec latency in EPPL calculation (Packet generation interval is 100 msec). Accordingly, Figure 16(b) shows that the LOS/OLOS/NLOS model has a higher EPPL than Friis-Nakagami model. Interestingly, it shows that relaying results in a lower EPPL than the case without relaying for both loss models. This is because, relaying has two contradictory impacts on the EPPL. On the one hand relaying improves PDR (Figure 15(a)), which reduces the number of dropped packets, hence it impacts positively in reducing EPPL. On the other hand, relaying increases the PRPL for a received packet, which negatively impacts on reducing the EPPL. Hence, it seems the overall EPPL depends on which factor dominates. However, as a dropped packet contributes more latency (100 msec) than a received packet (which is less than 10 msec) in the EPPL calculation, one can conclude that relaying has an overall positive influence for reducing latency in EPPL calculation of a loss model. Nevertheless, the overall EPPL is less than 80 msec, which is less than the packet generation time (100 msec).

4) PTV Vissim Traffic Car-Following Microsimulations (Milestone 2.2.1)

The car-following automated algorithm was accessed by conducting microsimulations in emergent traffic environments as created by VISSIM. This was done by creating a single-lane highway in VISSIM – based on a 4.0 km stretch of road near Greenville, SC, whereby the human-modeled drivers were tuned to replicate empirically measured time headways. Randomly mixed fleets of human-modeled and automated traffic were then initialized into the network and measured for energy and flow effects. Further details can be found in Quarterly Reports 6, 8, and 9, as well as in [7].

To accurately estimate the energy impacts of the MPC control, the finalized VISSIM microsimulations were processed in Autonomie, a state-of-the-art vehicle energy consumption model [19]. Vehicle models in Autonomie are Simulink-based and forward-looking, with a driver actuating virtual pedals to follow a drive cycle – speed as a function of time. An automated workflow was designed to load micro-simulation results (speed traces) and run large-scale Autonomie simulations using parallel computing in matter of few hours. The number of simulations can be scalable to 1 million.

Three powertrain configurations were used: conventional engine-powered vehicle (CV), electric vehicle (EV) and hybrid-electric (HEV). The HEV is a one mode power-split hybrid, a configuration similar to the one featured on the Toyota Prius. Each vehicle is of a midsize SUV class, and the component power and mass were sized for each vehicle to meet similar performance requirements, such as 0-60 mph time or ability to climb grades. In addition, the EV was sized to reach a 200 all-electric mile range. Efficiency and power density assumptions are based on DOE technology assumptions for current (2019) vehicles [20].

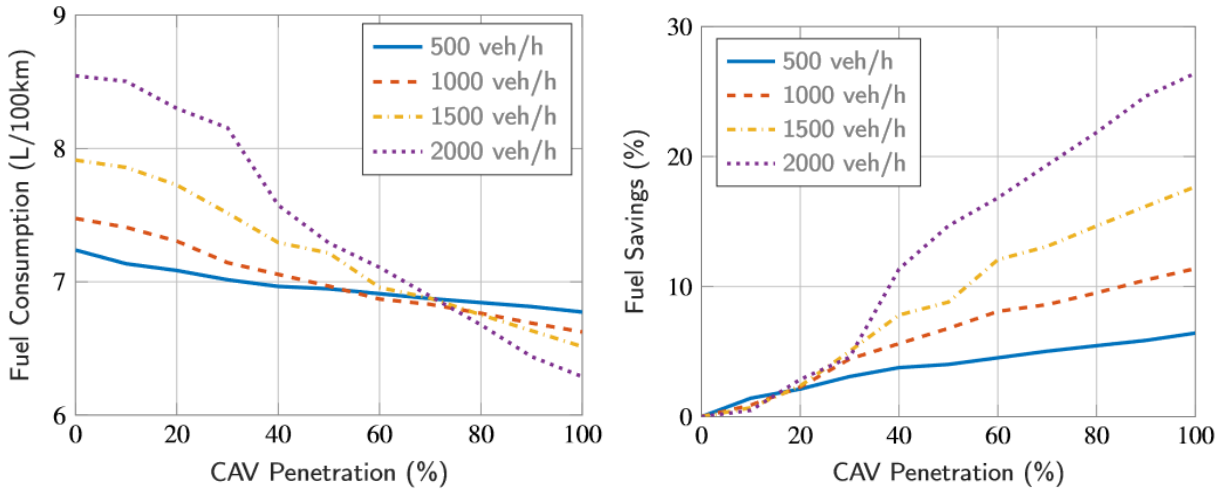

Figure 17: CV fuel consumption and fleet fuel efficiency improvements over the 0% CAV case at each input vehicle volume/hour.

Each {Volume, Penetration rate} scenario was simulated with each vehicle type in a homogenous fleet scenario (only one vehicle class and powertrain per scenario). Figure 17 shows the average energy consumption and average energy saving results of for the CV, as a function of penetration and volume. The average energy saving figure uses the energy consumption at 0% penetration for the same volume as a reference.

Higher penetration rates of the MPC control brings greater energy savings for the entire fleet. For example, 50% and 100% penetration in the high-volume scenario yields resp. 15 and 27% energy savings compared to the scenario with no MPC at all. It should also be noted that the savings are greater at higher volumes for a given penetration. This is because greater speed oscillations and more braking events occur when there

are more vehicles on the road, and as a result the baseline average energy consumption at high volume is higher than at low.

Energy saving trends are similar for the EV and HEV, as shown in Figure 18, but the magnitude is lower. The main reason behind this difference is regenerative braking: even in the most congested scenarios at 0% penetration, little friction braking is done for both the BEV and the HEV, and a large share of the braking energy is recovered by the battery instead, which it can then use for propulsion. In fact, much of the saving potential of hybridization is already achieved at 0% penetration: the HEV already consumes between 25% and 35% less fuel compared to the conventional at 0% penetration rates.

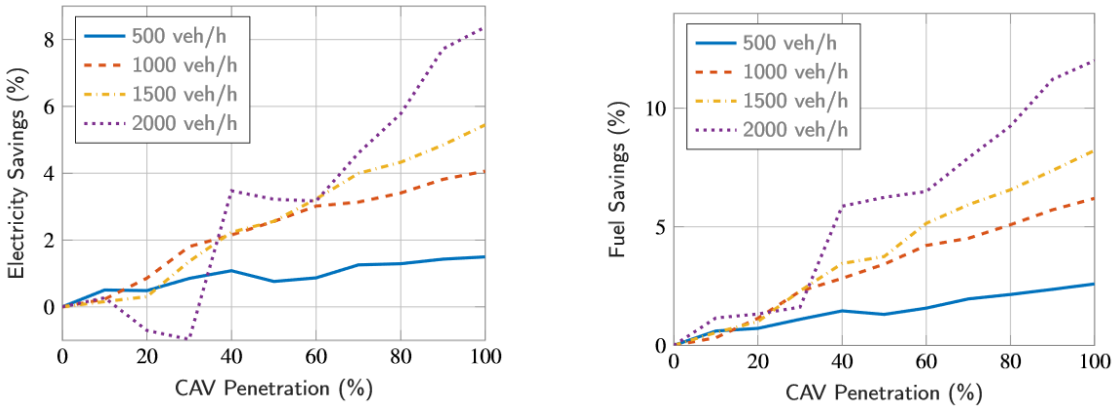

Figure 18: Fleet fuel efficiency improvements over the 0% CAV case at each input vehicle volume/hour for the EVs (left) and HEVs (right).

Finally, the effects of the automated vehicles on the surrounding traffic can be observed. We examine the traffic smoothening capabilities of the car following controller. Cell density plots are shown in Figure 19, in which shockwaves are depicted by high density regions of vehicles propagating backwards through the network over time – in the 0% case, shockwaves are present, but in the 30% case the shockwaves are dissipated.

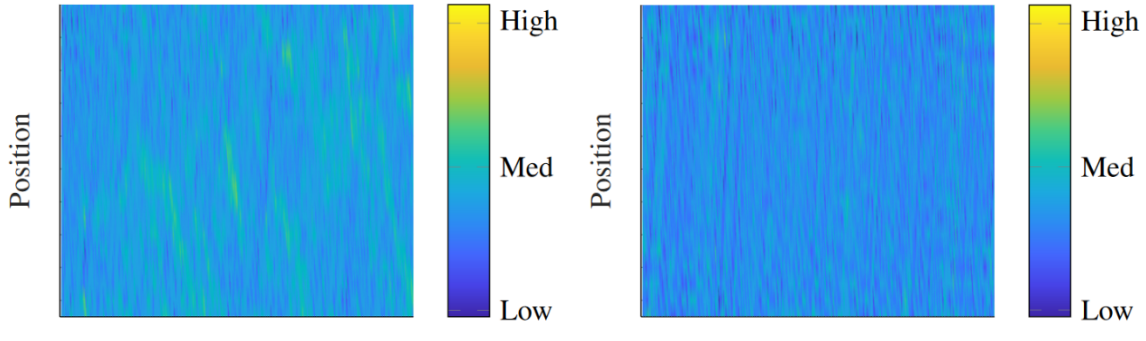

(a) 0% CAV penetration. (b) 30% CAV penetration.

Figure 19: Cell density plots showing dense groups of vehicles in the network at 0%, 30% CAV penetration. With the introduction of CAVs, shockwave effects were dissipated.

5) Non-Linear Programming Lane Decision Algorithm (Milestone 2.1.1)

a. Framework Overview

A mixed-integer quadratic programming approach to lane decision algorithm was presented in Section 3. Another student developed a nonlinear programming approach that got implemented in VISSIM microsimulations and is ready to be deployed on the experimental vehicles. This section summarizes this alternative formulation and implementation. Before discussing the control algorithm and framework, we will introduce some terminology and present a sample traffic topology (20). The mixed traffic consists of connected and automated vehicles (CAVs), as well as, human driven vehicles (HDVs). From the perspective of a given CAV c_i there are three different sets of vehicles, $\mathcal{C}_i$ the set of all CAVs c_p ($p \neq i$) communicating with CAV c_i, $\mathcal{F}_i$ the set of all object vehicles (OV) ov_q (both CAVs and HDVs) in the field of view (FOV) of CAV c_i, and $\mathcal{E}_i = \mathcal{C}_i \cup \mathcal{F}_i$ the extended neighborhood of CAV c_i.

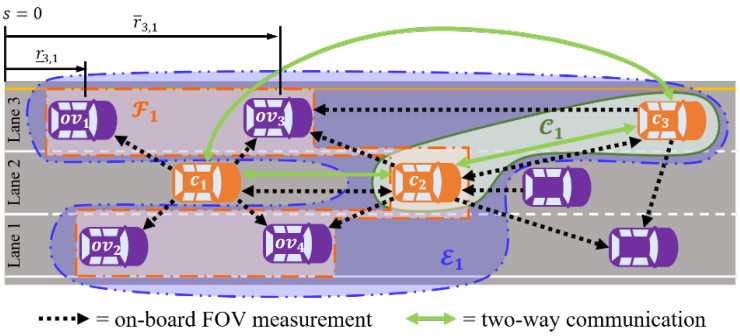

Figure 20: Sample traffic topology, where $\mathcal{C}_1 = \{c_2, c_3\}$, $\mathcal{F}_1 = \{ov_1, ov_3, c_2, ov_2, ov_4\}$, and $\mathcal{E}_1 = \{ov_1, ov_3, c_2, ov_2, ov_4, c_3\}$.

The control framework consists of four components, the object vehicle state prediction (OVSP) block, the reference speed assigner (RSA) block, the distributed model predictive control (DMPC) block, and the lower level vehicle motion dynamics block [4, 15, 16]. The control framework is outlined in Figure 21 and described in the following paragraphs.

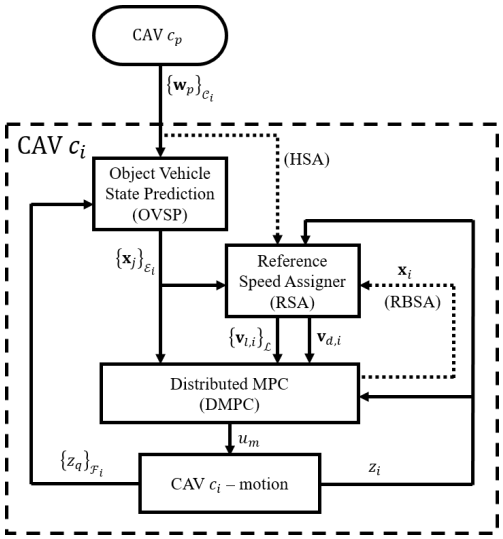

Figure 21: Block diagram of the optimal lane selection NLP distributed MPC framework

At each time step, CAV c_i obtains a set of measurements $\{z_q\}_{\mathcal{F}_i}$ containing information about each $ov_q \in \mathcal{F}_i$, as well as a set of shared information matrices $\{\mathbf{w}_p\}_{\mathcal{C}_i}$ containing shared information from each CAV $c_p \in \mathcal{C}_i$. This information is used by the OVSP block to obtain the set of state trajectories $\{\mathbf{x}_j\}_{\mathcal{E}_i}$ containing a predicted state trajectory for each $ov_j \in \mathcal{E}_i$. To predict the state trajectories of HDVs decoupled longitudinal and lateral linear prediction models and a Kalman filter are used [15, 16]. For CAVs, the information matrix $\mathbf{w}_p$ shared by each CAV c_p is assumed to contain the prior time step predicted plan, which is synchronized with CAV c_i's current planning time step via the methods in [15, 16]. The predicted state trajectories are then passed to the RSA block.

We implement two methods of reference speed assignment. The first method, rule-based speed assignment (RBSA), utilizes the predicted state trajectories of OVs, the current measurement z_i about CAV c_i, the prior time step predicted optimal state trajectory $\mathbf{x}_i$, and a set of rules to assign the reference speed v_l of a given lane l in the set of lanes $\mathcal{L}$ based on the speed of CAV c_i's immediate neighbors [4, 15]. The second method, harmonization-based speed assignment (HSA), utilizes the estimated current speed of vehicles in $\mathcal{F}_i$ and

shared information to assign $v_{l,i}$ based on the average speed of vehicles in the given lane l [4, 16]. After assigning a reference speed to each lane l, the RSA block (using either method) then assigns the vehicles own desired speed $v_{d,i} = \underset{v_l}{\operatorname{argmin}}(v_{l,i} - v_{do,i})$, where $v_{do,i}$ is the base desired velocity of CAV c_i assigned by a higher level route planner.

The DMPC block then takes as input the predicted state trajectories of each $ov_j \in \mathcal{E}_i$, the set of lane reference speeds $\{v_{l,i}\}_{\mathcal{L}}$ and desired speeds $\mathbf{v}_{d,i}$, and the current measurement z_i about CAV c_i to optimize a state trajectory over the prediction horizon. The cost function consists of four major components: the lane-dependent cost weighs the costs for tracking each lane; the lane-independent cost penalizes deviations from CAV c_i's egoistic objectives; the predictability cost penalizes deviations from the prior plan; and the input cost promotes smooth and comfortable control decisions [4, 15, 16]. For our specific implementation, a path intrinsic particle motion model is used for planning along with elliptical OV avoidance constraints. For a complete overview of constraints please see [16] and [17]. The control inputs from the first time-step are then passed to the lower level vehicle motion dynamics block and applied, while the planning process is repeated.

b. Results – Reference Speed Assigner Comparison

The simulated traffic network is comprised of a 5000m long straight three-lane link, with a single input node and single output node as shown in Figure 22. The input node is located on the left with the direction of travel to the right. For the first 30m of the link, vehicles are restricted from changing lanes, in order to prevent a vehicle from moving directly into the path of a neighboring vehicle that has not yet entered the network. The desired velocities of vehicles were distributed using the default speed distribution in VISSIM with a mean of approximately 87 km/hr.

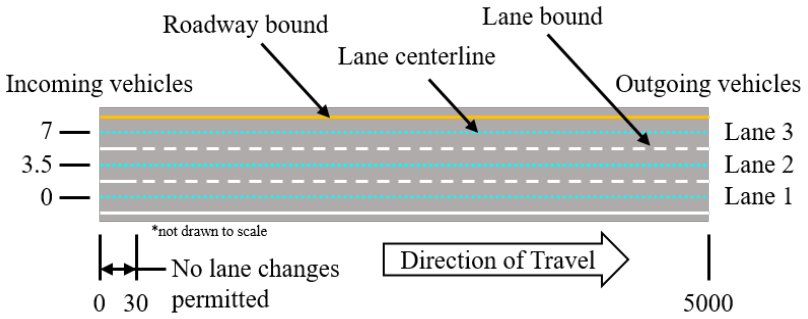

Figure 22: VISSIM traffic network.

Simulations were run for 30 minutes of simulation time with CAV penetration rates from 0 to 100% increasing in 10% increments and at low ($Q_L = 2000$ veh/hr), medium ($Q_M = 4000$ veh/hr), and high ($Q_H = 6000$ veh/hr) traffic demands. The network starts the simulation empty, therefore, for evaluation purposes we omit the time from the start of the simulation until the number of vehicles on the network reaches 90% of the maximum observed number of vehicles on the network. We will refer to the remaining simulation time as the evaluation duration. Human driven vehicles (HDVs) are assumed to follow the Wiedemann-99 psycho-spacing car-following model, and the default rule-based lane selection (RBLS) algorithm of VISSIM, which was originally developed by Spurmann [18]. For all future discussions, the baseline scenario will be 0% CAV penetration at the respective traffic demand with ALL vehicles being HDVs.

We define the percent reduction in fuel consumption $FC\%$ as follows [4, 16]:

$$FC\% = 100\left(1 - \frac{FC}{FC_b}\right),$$

where FC is the average fuel consumption rate for the given scenario, and FC_b is the average fuel consumption rate for the associated baseline scenario. As the average velocity from scenario to scenario changes, we will also introduce the travel time adjusted percent reduction in fuel consumption $AFC\%$:

$$AFC\% = FC\% - 100\left(\frac{RFC - RFC_b}{FC_b}\right),$$

where RFC and RFC_b are the fuel consumption rates required to maintain a constant velocity at the observed average velocity for the given scenario and the baseline scenario, respectively.

The percent reduction in fuel consumption results for simulations with CAVs utilizing either RBSA or HSA are presented in Figure 23 [4]. It can be seen in Figure 23 that at low and medium traffic demand the fuel consumption performances of the NLP lane decision algorithm for both the RBSA and HSA cases are comparable. On the other hand, at low penetrations and high traffic demand there is a significant difference between the RBSA case and the HSA case, with the HSA method outperforming the RBSA approach by around 6%. The fuel consumption performance of the two approaches converges as the CAV penetration is increased, with both approaches consuming fuel at a rate around 32% lower than the baseline scenario when adjusting for travel time.

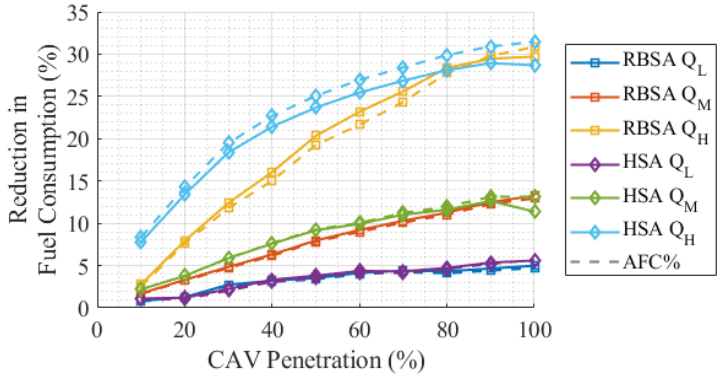

Figure 23: Percent reduction in fuel consumption of the entire fleet (CAVs and HDVs) compared to 0% CAV penetration at low, medium, and high traffic demands, for both the RBSA and HSA cases.

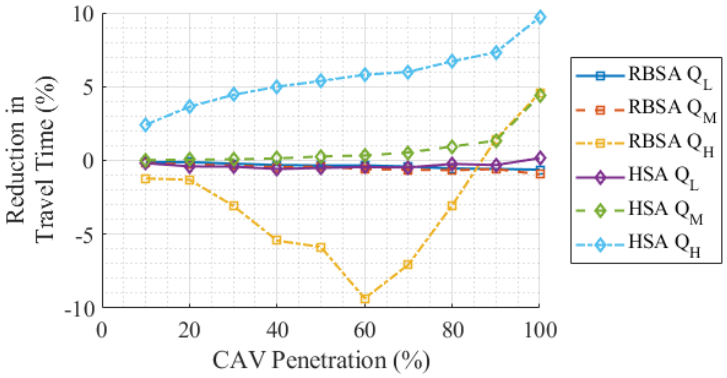

Figure 24: Percent reduction in travel time of the entire fleet (CAVs and HDVs) compared to 0% CAV penetration at low, medium, and high traffic demands for both the RBSA and HSA cases.

Figure 24 presents the travel time results, where the percent reduction in travel time is calculated in a similar manner to $FC\%$ [4]. At medium Q_M and high Q_H traffic demands, the HSA approach results in a significant improvement over the RBSA approach. At medium traffic demand and penetrations over 70% CAVs, the HSA approach is able to reduce travel time significantly compared to the baseline (1 to 4.5% reduction), whereas the RBSA approach marginally increases the travel time compared to the baseline (appx. -1% reduction). At high traffic demand and all CAV penetrations the HSA approach is able to realize a 2 to 7% reduction in travel time compared to the baseline scenario, whereas the RBSA approach results in a 1 to 9% degradation in travel time performance at penetrations below 90%. At 90% CAV penetration and above the RBSA case is able to reduce the travel time by 1 to 5%. The HSA case results in a 5% to 15% improvement in travel time reduction compared to the RBSA method at high traffic demand.

The difference in performance between the two methods is a result of the underlying goal of either RSA method. The HSA attempts to track the average speed of neighboring traffic, while the RBSA attempts to track the velocity extremes of neighboring vehicles. Due to the way the rules in the RBSA are designed,

this results in tracking the lower extreme in dense traffic. Therefore, at low to moderate CAV penetrations (10 to 60% CAVs), when HDVs cause a significant number of braking disturbances, this results in slower moving traffic. However, RBSA CAVs do have smoother control actions than HDVs, therefore once a critical CAV penetration is obtained (60% CAVs), the smoothing effect of CAVs is more prominent and the travel time performance begins to improve.

c. Results – Impacts of Optimal Lane Selection

In order to isolate what portion of these benefits are due to optimal lane selection, we compared the proposed 2D maneuver planning non-linear program (NLP) based distributed MPC (DMPC) framework to a longitudinal DMPC with VISSIMs internal rule-based lane selection (RBLS) for lateral control. To clarify, the same basic formulation for both DMPCs is utilized, however, for the RBLS DMPC only the desired acceleration (a_d) is applied. For lateral control and lane selection, the RBLS DMPC CAV applies the desired lane angle (ψ_d) calculated by VISSIMs internal rule-based algorithm. Further, the reference speed assigner was modified for the RBLS DMPC such that:

$$v_l = \begin{cases} \hat{\mu}_l & \text{if CAV } c_i \text{ occupies lane } l \text{ or a signal is obtained that CAV } c_i \text{ is changing to lane } l \\ \epsilon & \text{otherwise} \end{cases},$$

where v_l is the lane reference speed, $\hat{\mu}_l$ is the estimated average speed of traffic in lane l, and ϵ is a small number. As the primary differentiator between the two DMPC versions is the lane selection algorithm, we will refer to the proposed DMPC version as optimal lane selection (OLS) DMPC, and the reference DMPC with rule-based lane selection as RBLS DMPC.

We begin by analyzing the travel time results presented in Figure 25 [16]. At low traffic demand and all CAV penetrations, as well as, at medium traffic demand and low to moderate CAV penetrations (<75%), the RBLS and OLS DMPC versions match the travel time performance of the baseline (0%) scenario. At high CAV penetrations (>75%), both DMPC versions reduce the average travel time of traffic, with the OLS version marginally outperforming the RBLS version. At high traffic demand, the OLS DMPC version significantly outperforms the baseline and RBLS version at all CAV penetrations. Conversely, the RBLS framework only outperforms the baseline at moderate to higher CAV penetrations (≥25%). We will next investigate the fuel consumption implications of the two DMPC versions. Figure 26 presents the $FC\%$ and $AFC\%$ for both DMPC versions as a function of CAV penetration at the three traffic demands Q_L, Q_M, and Q_H [16]. In general, there is not a significant difference in the fuel consumption rate of the RBLS and OLS versions. The largest observed difference is at a traffic demand of Q_H and 25% CAV penetration, where the OLS DMPC version improves $FC\%$ by almost 3% more than the RBLS version and $AFC\%$ by almost 4%. As penetration increases, at high traffic demand Q_H, the performance of the two DMPC versions converges. The reason the OLS DMPC does not improve $FC\%$ and $AFC\%$ significantly compared to the RBLS DMPC, is that there is minimal room for improvement. In both cases, the goal of the controller is to track reference speeds while minimizing accelerations, therefore, based on the reference speed assigner, the

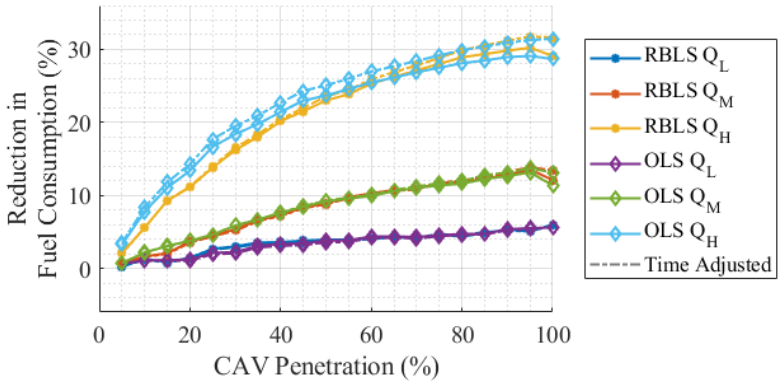

Figure 26: Percent reduction in fuel consumption of the entire fleet (CAVs and HDVs) compared to 0% CAV penetration at low, medium, and high traffic demands, for both the RBLS and OLS DMPC versions.

optimal solution without disturbances would result in the RFC. To illustrate this, we define $\Delta RFC\%$, the percentage difference of the observed fuel consumption rate to the required fuel consumption rate, as:

$$\Delta RFC\% = \frac{FC - RFC}{FC_b}$$

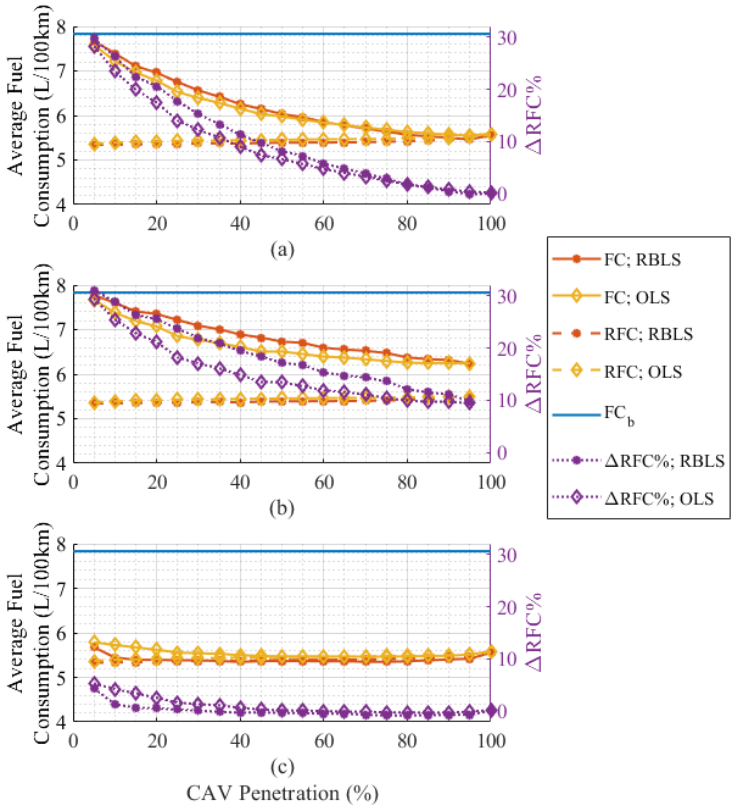

Figure 27: FC and $\Delta RFC\%$ of (a) the entire fleet (CAVs and HDVs) (b) human driven vehicles (HDVs), and (c) connected and automated vehicles (CAVs) at low, medium, and high traffic demands, for both the RBLS and OLS DMPC versions.

We present the fuel consumption rate and $\Delta RFC\%$ results for Q_H as an example in Figure 27 [16]. This figure separates the average fuel consumption into different subsets of the vehicle population, specifically, the entire mixed fleet (both CAVs and HDVs) in Figure 27(a), only the HDV population in Figure 27(b), and only the CAV population in Figure 27(c). When referencing the CAV population in Figure 27(c), it can be seen that for both DMPC versions there is a negligible difference between RFC and FC above 50% CAV penetration. At CAV penetrations below 50%, the RBLS version actually results in marginally reduced FC for CAVs than the OLS framework. However, as seen in Figure 27(b), the OLS version results in a reduction in fuel consumption of HDVs, which make up the majority of traffic, compared to the RBLS version. This results in a marginal reduction in fuel consumption of the entire mixed fleet (see Figure 27(a)) for the OLS framework compared to the RBLS framework at CAV penetrations below 50%.

6. Collaborative Guidance (Milestone 2.3.1)

While the algorithms described in Sections 2 and 3 shared information between CAVs, they were fully decentralized in their fleet solutions; that is, they consider the surrounding CAVs' trajectories as fixed and optimize their own objectives. In the collaborative guidance stipulated in Milestone 2.3.1, each vehicle acts to improve the group's objective via additional information exchange. Section 6-a reviews collaboration in a single lane and Section 6-b deals with a different approach for multi-lane collaborative guidance. In both cases, centralized optimization is used as a high-performing benchmark.

a. Collaborative Single Lane Guidance

The single-lane collaborative algorithm begins as a special case of the hierarchical system of Section 6-b. It is thus an eco-driving controller rather than a car-following controller; its objective does not track a gap relative to the PV but instead minimizes the energy consumed by the electric powertrain over the trip. First, each CAV in the string computes its parabolic reference speed trajectory. This trajectory is then communicated to neighboring vehicles. Finally, each vehicle solves a group optimization considering its immediate neighbors and applies only its own control input. In this way, the CAVs attempt to reduce not only their own energy consumption but also those of nearby vehicles. Reference [3] and Quarterly Report 9 describe this algorithm along with other approaches that were compared in MATLAB simulations.

8-vehicle CAV strings following a lead vehicle were simulated, where the leader adhered to the WLTC High or Low cycle. The WLTC Low results are shown in Figure 28. The classical and reactive adaptive cruise control (ACC) exhibited a tradeoff between total energy and string length depending on its time headway setting. The position constrained shrinking horizon controller (PCSHC) used a constant acceleration assumption for the PV to analytically determine the optimal control. While it smoothed the first CAV's trajectory, it was string unstable and consumed more energy over the string compared to the hierarchical optimal control algorithms. DHC denotes the decentralized approach described in Section 6-b, applied to a single lane. In Centralized Hierarchical Control (CHC) the receding horizon part of the problem was solved as a single optimization for all agents, which followed that optimization's result exactly. Cooperative Hierarchical Control (CoHC) is the distributed approach discussed previously. It delivered nearly as low energy consumption as CHC and resulted in the lowest string length of the algorithms tested. In a single lane, the chief benefit of collaboration was in string length rather than energy consumption. Reference [3] provides additional results, including those obtained using the WLTC High cycle.

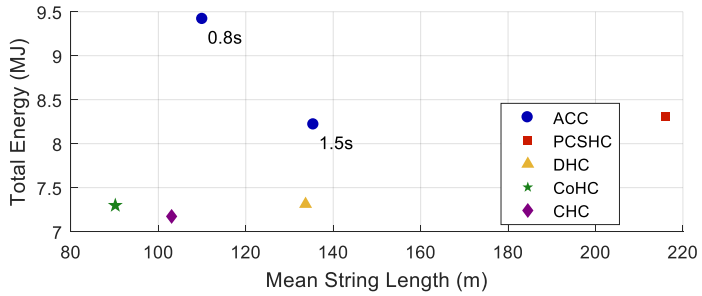

Figure 28: The string length and total EV energy consumption of several eco-driving algorithms in an 8-vehicle, drive cycle-based MATLAB simulation.

b. Collaborative Multi-Lane Guidance

The optimization in multi-lane situations is more complex. Therefore, a different collaboration approach was developed in [1] that only solves for a single CAV's control move per optimal control problem. Noticing that the decentralized algorithm's group solution depends on the order in which the vehicles compute their trajectories, the Prioritized algorithm dynamically seeks better orderings to improve the group objective. Each CAV first solves a nominal problem in which all other CAVs are assumed to yield to it. The norms of these problems' gradients at optimality are then used to measure each CAV's sensitivity to additional collision avoidance constraints. More sensitive vehicles are then prioritized such that less-sensitive agents yield to more sensitive ones. Centralized navigation was also implemented, although its computation time would make it impractical for real time implementation.

The simulation scenario required 3 CAVs to navigate around an obstacle as shown in Figure 29. This emphasizes the role of collaboration since the agents must adjust their speeds and resolve conflicts to reach their goals. The distributed Prioritized controller reduced energy consumption by 6.7% relative to the decentralized baseline, while the less practical centralized approach reduced energy use by 8.6% as shown in Figure 30. Further research on this topic is needed to determine the extent to which these energy improvements apply in other scenarios. It is likely that collaboration is especially critical in denser traffic and bottlenecks like the one examined here.

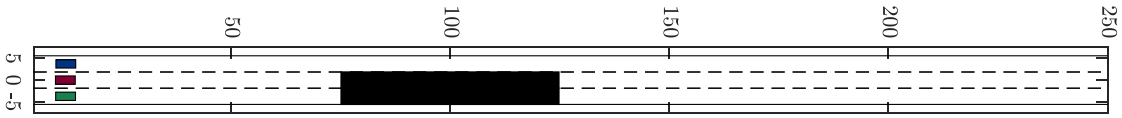

Figure 29: The scenario used to evaluate the collaborative multi-lane algorithm.

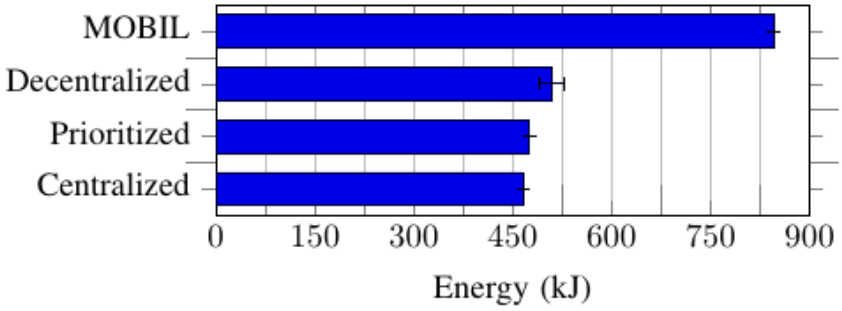

Figure 30: Energy consumption improvement from distributed collaboration and centralized guidance.

7) Experimental Vehicle Instrumentation

To accomplish the goal of this project, the test vehicles required pedal and steering actuators to command the vehicle autonomously, and low-level controllers to convert the motion commands from the high-level controller to pedal and steering wheel operations.

7.1 Vehicle Instrumentation

Testing in this project consisted of one electric vehicle (Nissan Leaf) and one gasoline engine vehicle (Mazda CX-7). Both vehicles were not equipped with automated driving capabilities from the manufacturer, so they were modified to execute the commands from the high-level controller autonomously. The modifications include adding necessary sensors, actuators, and designing control algorithms. The relationship between the sensors, actuators and controls in the low-level controller is shown in Figure 31.

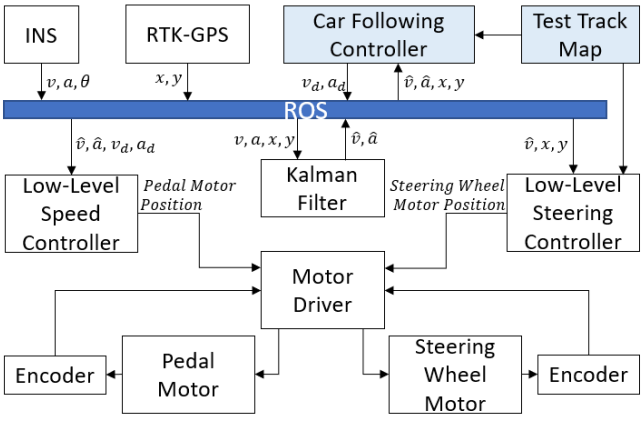

Figure 31: Structure of low-level controller.

The pedal and steering wheel actuators were specially designed. They share a similar design for both vehicles. Figure 32 left shows the structure of the pedal actuator. The actuator was designed to only push either the accelerator or brake pedal, and so features a release mechanism which releases the engaged pedal before actuation switches to the other. This is accomplished through levers 2 and 3, which have different rotation directions: lever 2 is attached to the output shaft of electric motor 1, whereas lever 3 is attached to another shaft that

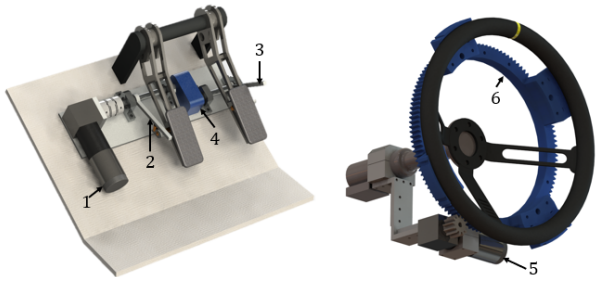

Figure 32: Specially designed actuators for pedal and steering wheel.

is parallel to and connected to the motor shaft via gear drive 4. A lever can push down the corresponding pedal by applying force on a small cylinder that is protruding from the side of the pedal, but the lever itself is not rigidly fixed to the pedal. Thus, when lever 2 rotates down, the brake pedal is pressed, and the accelerator pedal is released - and vice versa. Figure 32 right shows the structure of the steering wheel actuator. The electric motors 5 drives the gear ring 6 that is mounted behind the steering wheel so that the steering wheel can be rotated. The instrumented vehicles with the actuators and sensors are shown in Figure 33.

Figure 33: Instrumented test vehicles.

7.2 Low-Level Longitudinal Controller Design

Longitudinal control of the vehicle is achieved by directly controlling the brake and accelerator pedals. However, the dynamics from pedals to vehicle motion is highly non-linear due to the existence of internal combustion engine and transmission or batteries, and the calibration map of the engine, transmission or the battery is not available from the factory. Those factors make the implementation of solely a traditional controller or a data-driven artificial neural network (ANN) controller difficult. Thus, the two approaches are fused to combine a data-driven feedforward controller with a classical PID feedback controller to solve the speed and acceleration tracking problem.

A Pure Pursuit controller was implemented for the experimental vehicles to track the designated path of the test track. The steering input ψ to the vehicle is computed with the location of the target point l_d and the angle α between the vehicle's heading direction and the look-ahead direction

$$\psi = k \cdot tan^{-1}\left(\frac{2Lsin\alpha}{l_d}\right)$$

where l_d is the look ahead distance given by

$$l_d = {l_d}^{min} + k_l v$$

where k_l and ${l_d}^{min}$ are tunable gain and minimum look-ahead distance parameters.

7.3 Low-Level Longitudinal Controller Performance

Both experimental vehicles were calibrated to follow a short square-wave speed profile while driving on a rough road with notable grade. A dynamic target generator was created based on the IDM, which calculates desired speed and desired acceleration from the speed profile.

$$a_d = a_0\left(1 - \left(\frac{v}{v_0}\right)^4\right)$$

$$v_d = v + a_d \Delta t$$

Here, $a_0 = \pm 2.0 m/s^2$ is the maximum acceleration, and v_0 is the target speed from the square-wave-shaped profile. The PID controllers were tuned to reject the road disturbance without notable overshoot.

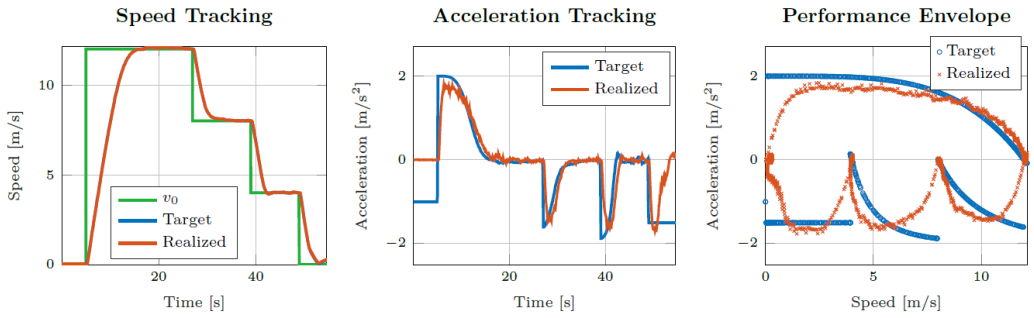

Figure 34: Nissan Leaf speed profile tracking performance.

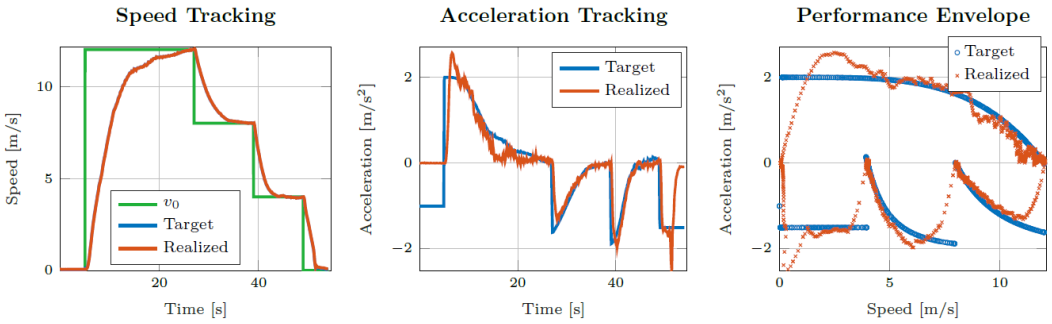

Figure 35: Mazda CX-7 speed profile tracking performance.

The result is shown in Figures 34 and 35. The combined controller showed fast response and small tracking error. The steady state speed tracking error was $\pm 0.06 m/s$ for both vehicles. The acceleration tracking was also accurate, where the performance envelope shows that the acceleration tracking was acceptable over the entire domain of velocity.

The calibrated controllers on both vehicles were combined with a high-level IDM controller to test their performance under a more comprehensive car following scenario. The physical vehicle followed a virtual vehicle that tracked US06 drive cycle in this test. This test was conducted on the test track as introduced in Section 9. The result is shown in Figures 36 and 37.

In the figures, the black solid curves show the speed and acceleration of the ego vehicle obtained from a simulation. The simulation utilized a simple kinematic model to calculate the motion of the ego vehicle in

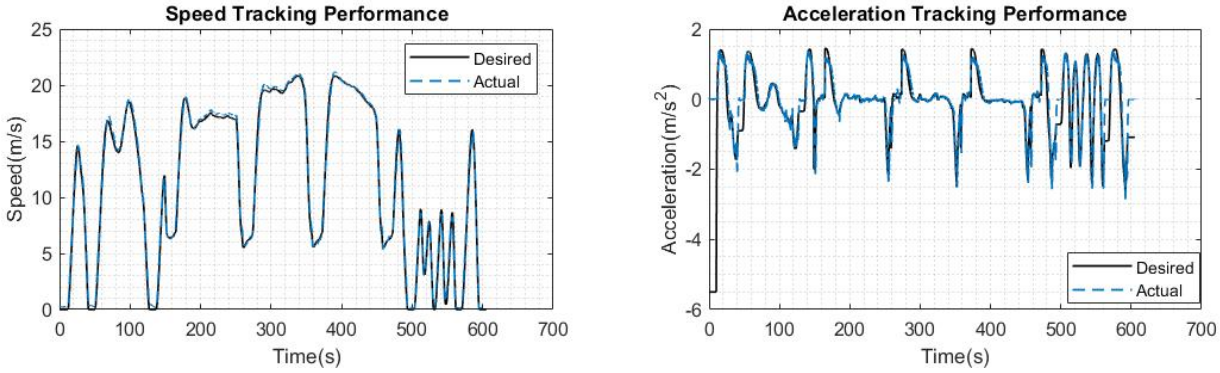

Figure 36: Nissan Leaf car following performance.

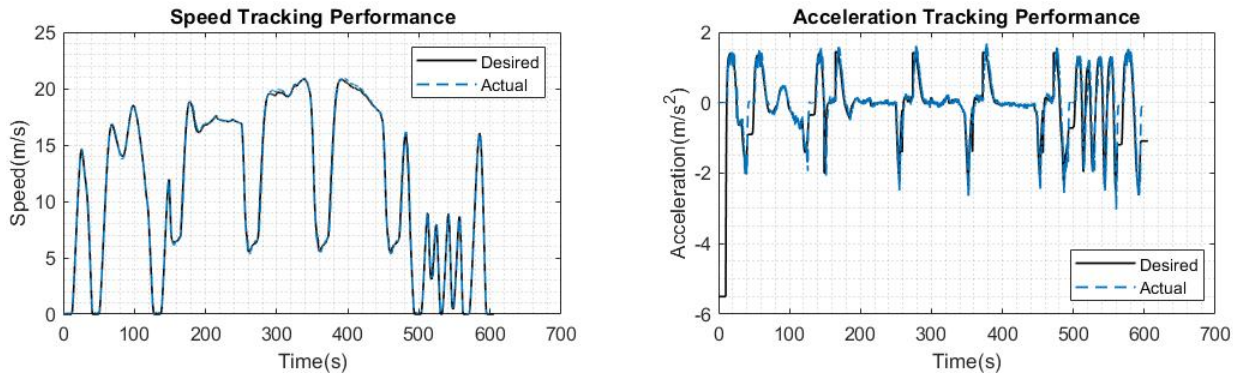

Figure 37: Mazda CX-7 car following performance.

ideal environment. Thus, the closer the actual curve is to the desired curve, the better performance the controller can offer. The figures show that the actual speed and acceleration curves are almost overlapped with the desired ones, which indicates a satisfactory controller performance. In this test, the average absolute acceleration tracking error was smaller than 0.2 m/s^2 for both vehicles.

8) Vehicle-in-the-Loop Experiments (Milestones 3.1.1, 3.1.2, 3.2.1)

Vehicle-in-the-loop (VIL) is our proposed automated driving virtual simulation in which a physical vehicle (ego) is embedded into a traffic scenario with the goal of evaluating performance of such cyber-physical systems in a realistic manner without compromising safety. This aspect is one of the novel contributions of the project that has broader impact in testing automated vehicles. Driver perspective is depicted in Figure 38. The vehicle positions are mapped directly to the simulation environment to embed it in simulation in real-time by communicating its (x, y, v, θ) tuple. The results are summarized below, and more complete details can be found in Quarterly Report 10, as well as [14].

To accommodate for safety considerations on the test track due to road geometry, speed limits and U-turns were imposed. To impose in vehicle guidance, first recall particle kinematic equations of constant acceleration,

$$a_c\, ds = v\, dv \rightarrow v^2 = v_0^2 + 2a_c\,(s - s_0) \tag{11}$$

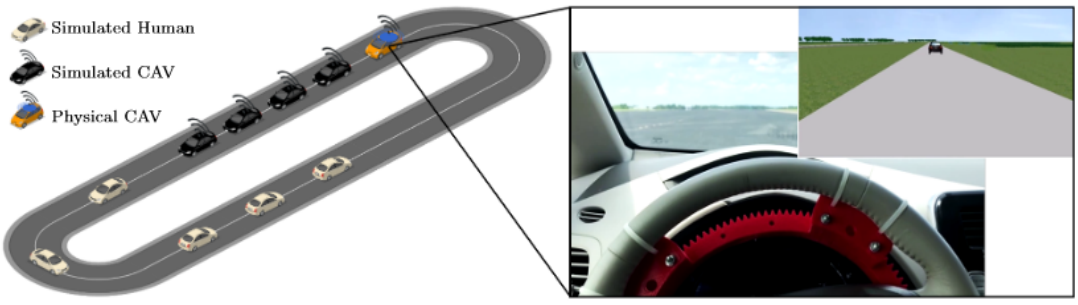

Figure 38: Visualization of the vehicle-in-the-loop environment from the driver perspective in both simulation and reality. The physical vehicle is embedded into a virtual environment and interacts with virtual drivers.

where $a_c = -2.0\text{m/s}^2$ is chosen as a comfortable deceleration to reach the U-turn velocity from straight-away velocity. The quantity δs then describes the distance away from the U-turn speed limit $\bar{v}_1$ needed to slow down from straight-away speed limit $\bar{v}_0$.

$$\delta s = \frac{\bar{v}_1^2 - \bar{v}_0^2}{2a_c} \tag{12}$$

For the WIE and IDM controllers, switching control can then be applied when within δs as

$$u^+ = \min\{u,\ a_c\} \tag{13}$$

where u is the control of the WIE or IDM continuous model, and u^+ is the control command to apply when approaching the U-turns. This logic limits the control to only engage in the most conservative acceleration that occurs due to either car-following or velocity maintenance.

For the MPC, a constraint limits maximum velocity for each optimization stage. This poses challenges because the MPC optimization horizon is a function of time, whereas speed limit transitions are a function of distance instead.

An approximation is made to convert the velocity constraint to a function of time using an estimate of the ego's speed trajectory. In this case, a constant velocity is assumed in the speed estimate $\tilde{v}(i) = v,\ i = 0, \ldots, N$. The position estimate then follows as $\tilde{s}(i+1) = \tilde{s}(i)+\tilde{v}(i)\Delta t_h$. Combining with Eqns. (11, 12), the following can then be used to define the MPC moving velocity constraint with s_l describing the current distance from the speed limit.

$$\overline{v}(i) = \begin{cases} \overline{v}_0 & \tilde{s}(i) < s_l \\ \sqrt{\overline{v}_0^2 + 2a_c\left(\delta s - (s_l - \tilde{s}(i))\right)} & \tilde{s}(i) < \delta s + s_l \\ \overline{v}_1 & \tilde{s}(i) \geq \delta s + s_l \end{cases} \tag{14}$$

Similar approaches can follow for the moving velocity constraint when approaching a higher velocity speed zone.

A PTV VISSIM microsimulation environment was set up, which comprised of a single-lane circuit of 74 vehicles. The VISSIM human-driver model controlled all simulated vehicles, with the exception of the MPC-C scenario, in which a string of 5 simulated CAVs plus the ego CAV were controlled by the MPC. The EPA US06 and EPA UDDS drive cycles were also used to set the velocity profile of the PV, where the velocity trajectories of the cycles were scaled down by 40% and 15%, respectively, because of the speed limits at the test track (please see Figure 41).

Energy estimation was accomplished using calibrated mass-airflow and battery sensors for the combustion engine Mazda and the electric vehicle Nissan.

The results for the VIL experiments with the 3 simulation variants are given for the two vehicles. Here, the high-level controller types of Wiedemann 99 (WIE), Intelligent Driver Model (IDM), Unconnected MPC (MPC-U), and Connected MPC (MPC-C) were examined for both their flow and energy impacts.

Table 2: Mazda-combustion microsimulated experimental controller performance

	WIE	IDM	MPC-U	MPC-C
Travel Time	24' 01"	23' 45" -1.1%	24' 00" -0%	23' 34" -1.9%
Avg. Headway [s]	3.47	5.73 +65.1%	3.32 -4.3%	2.75 -20.7%
Avg. Gap [m]	28	59 +111%	37 +32%	28 +25%
Max. Gap [m]	83	144 +73%	112 +35%	74 -11%
Net Fuel [L]	2.556	2.174 -15%	2.241 -12%	1.978 -24%

Table 3: Nissan-electric microsimulated experimental controller performance

	WIE	IDM	MPC-U	MPC-C
Travel Time	23' 49"	23' 49" -0%	23' 40" -0.9%	23' 36" -1.9%
Avg. Headway [s]	3.96	5.81 +46.7%	2.93 -26.0%	2.82 -28.8%
Avg. Gap [m]	27	62 +130%	31 +16%	32 +21%
Max. Gap [m]	76	151 +99%	96 +26%	82 +8%
Net Energy [kwh]	4.090	3.730 -8.8%	3.766 -7.9%	3.247 -20.6%

The MPC offered energy efficiency improvements over the WIE human-like driver for both vehicles. MPC-U reduced energy usage by 12% and 8% for the Mazda and Nissan, whereas MPC-C reduced energy usage by 23% and 21%. Additionally, it did not sacrifice realized time headway, unlike the IDM cruise controller.

Figures 39, 40 depict the position trajectories of each vehicle over time. One can observe stop-and-go behavior by the ripples in the position trajectories, which is detrimental to the energy economy of the fleet of vehicles. As opposed to the WIE scenario, the CAV string attenuated disturbances of the traffic and subsequently smoothed the driving of the vehicles behind. It was found that the MPC-C scenario improved fuel usage by 4.5% on average, the MPC-U scenario improved fuel usage by 0.4% on average, and the IDM *worsened* their fuel usage by 0.9%. By this, automated vehicles and connectivity have the potential to provide secondary benefits for improving the energy usage of neighboring traffic.

Likewise, for the US06, the MPC showed significantly improved energy economy over the WIE human-like driver. Overall, the MPC improved the Mazda energy performance by 26% and 32% in the unconnected and connected variants, while the MPC improved the Nissan energy performance by 17% and 25% for the unconnected and connected variants.

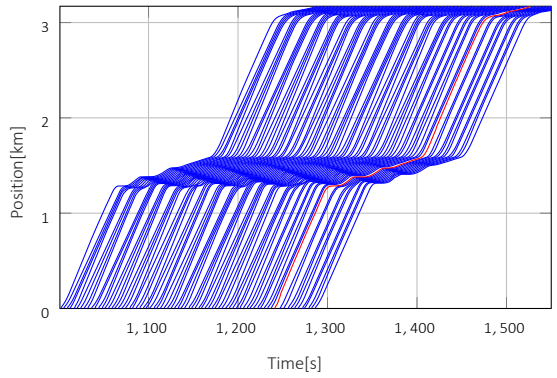

Figure 39: WIE position trajectories over time for the virtual human traffic (blue) and ego vehicle (red) for lap 5.

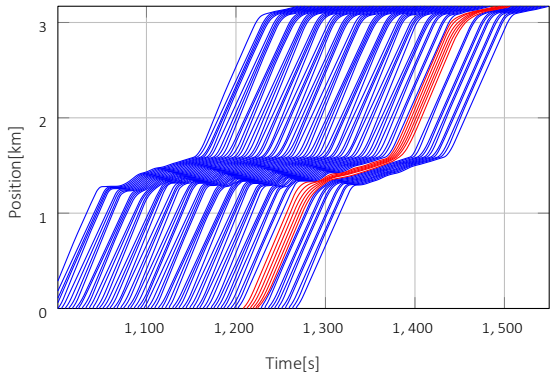

Figure 40: MPC-C position trajectories over time for the virtual human drivers (blue) and the MPC connected string (red) for lap 5. The ego is the backmost MPC vehicle.

The UDDS saw markedly improved energy economy as well. Overall, the MPC improved the Mazda energy performance by 14% and 24% in the unconnected and connected variants, while the MPC improved the Nissan energy performance by 25% and 34% in the unconnected and connected variants.

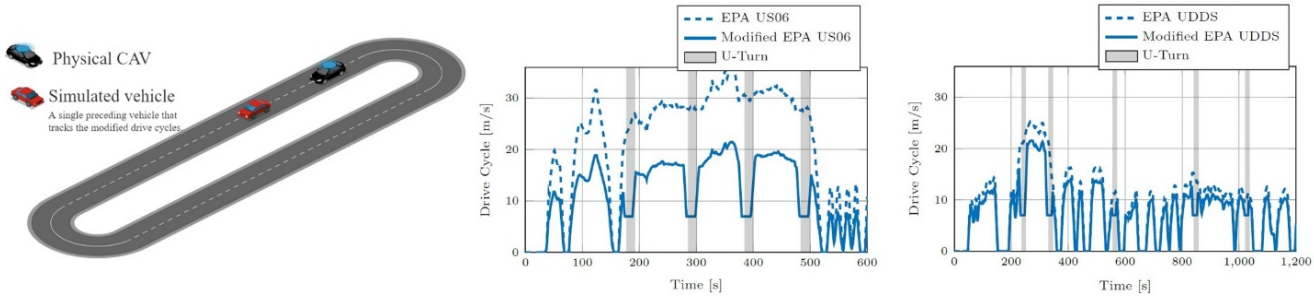

(a) US06 velocity profile

(b) UDDS velocity profile

Figure 41: Modified EPA drive cycle experimental velocity profiles used for the PV.

Table 3: Mazda-combustion: US06 controller performance

	WIE	IDM	MPC-U	MPC-C
Travel Time	9’ 20”	9’ 33” +2.3%	9’ 20” 0%	9’ 26” +1.1%
Avg. Headway [s]	2.45	6.23 +154.3%	2.64 +7.8%	2.66 +8.6%
Avg. Gap [m]	23	35 +52%	26 +13%	23 0%
Max. Gap [m]	40	93 +133%	77 +93%	88 +120%
Net Fuel [L]	1.006	0.840 -17%	0.746 -26%	0.684 -32%

Table 4: Nissan-electric: US06 performance[1]

	WIE	IDM	MPC-U	MPC-C
Travel Time	8’ 39”	8’ 39” 0%	8’ 38” 0%	8’ 39” 0%
Avg. Headway [s]	2.14	5.80 +171.0%	2.76 +29.0%	2.58 +20.6%
Avg. Gap [m]	24	38 +58%	28 +17%	25 +4%
Max. Gap [m]	42	92 +119%	78 +86%	82 +95%
Net Energy [kwh]	1.286	1.230 -4%	1.064 -17%	0.963 -25%

Table 5: Mazda-combustion: UDDS controller performance

	WIE	IDM	MPC-U	MPC-C
Travel Time	22’ 33”	22’ 36” +0.2%	22’ 35” +0.1%	22’ 36” +0.2%
Avg. Headway [s]	3.39	5.94 +75.2%	2.85 -15.9%	3.53 +4.1%
Avg. Gap [m]	16	22 +38%	16 0%	20 +25%
Max. Gap [m]	46	99 +115%	83 +80%	70 +52%
Net Fuel [L]	1.370	1.329 -3%	1.175 -14%	1.048 -24%

Table 6: Nissan-electric: UDDS controller performance

	WIE	IDM	MPC-U	MPC-C
Travel Time	22’ 33”	22’ 35 +0.1%	22’ 34” +0.1%	22’ 34” +0.1%
Avg. Headway [s]	4.22	4.39 +4.0%	2.51 -40.5%	3.15 -25.4%
Avg. Gap [m]	16	22 +38%	15 -6%	19 -19%
Max. Gap [m]	43	111 +158%	85 +98%	79 +84%
Net Energy [kwh]	1.855	1.639 -12%	1.389 -25%	1.221 -34%

[1] Nissan Electric modified US06 results were shortened to the first 520s due to loss of some OBD-II data.

9) OBD-II energy measurement methods (Milestones 3.1.1, 3.1.2, 3.2.1)

An iOS app was created to pair with the On-Board Diagnostics (OBD-II) port of the vehicles with 29-bit ISO 15765-4 CAN protocol as in [21-22]. The implemented iOS app connects to commercial WiFi OBD-II dongles supporting the ELM327 chip [26], as depicted in Figure 42 and 43(a). The app also collects the iOS device's locational/GPS and timestamp data so that OBD-II readings could be correlated with simulation. Table 7 summarizes all this extra data. The collected data are available in a Comma Separated Values file format for further off-line data analysis. All the OBD datasets are also aggregated based on Unix timestamps. The app was extended to read the combustion engine Mazda CX7's 11-bit CAN protocol, as depicted in Figure 43(b), and the electric motor Nissan Leaf's unstandardized protocol, as depicted in Figure 43(c).

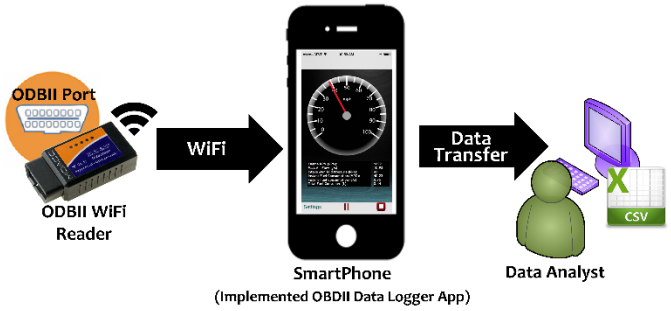

Figure 42: Functional architecture of the developed iOS OBD Logger App [21].

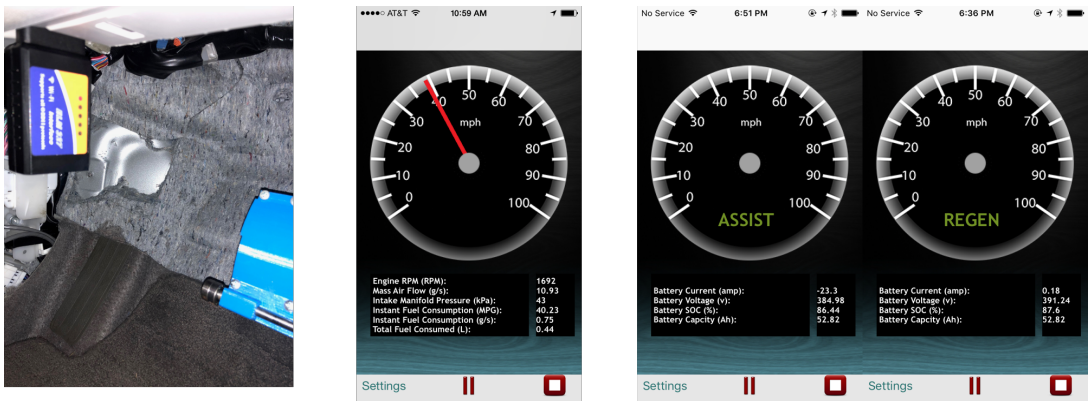

(a) (b) (c)

Figure 43: (a) An ELM327-based WiFi OBD-II reader attached to our test vehicle. The user interface showing real-time data of our test vehicles: (b) Mazda CX-7 2009 with gasoline engine, and (c) Nissan Leaf 2011 electric vehicle (REGEN denotes Regenerative Braking and ASSIST denotes Torque Assist mode).

Table 7. The extra data collected from the sensors of the iOS device for both experimental CAVs.

Data Name	Data Type and Unit	Collection Method	Sampling Rate
Timestamp	Continuous (UNIX)	iOS device sensor	1 Hz max
Vehicle Speed	Continuous (kph)	iOS device sensor	1 Hz max
Vehicle Orientation	Continuous (degree)	iOS device sensor	1 Hz max
Vehicle Position (GPS Latitude & Longitude)	Continuous (°)	iOS device sensor	1 Hz max
Vehicle Altitude	Continuous (m)	iOS device sensor	1 Hz max

A custom procedure was programmed to increase the default data sampling frequency of the ELM chip. In total, data was collected from the Mazda at a rate of 8hz, and data was collected from the Nissan at a rate of 4hz. This was accomplished by i) Sending "Carrier Return" to ELM327 instead of re-sending the exact previous command each time, ii) Programming the ELM327 not to wait 200 ms after each "Carrier Return" command, and iii) Sending the number of lines that ELM should expect to receive; as a result, after receiving the pre- defined number of lines, the ELM stops looking for new data. Figure 44 shows a typical ELM327 request and response.

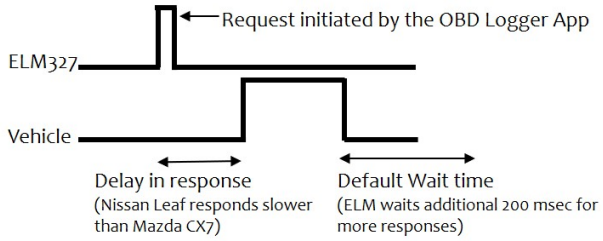

Figure 44: The default timing of ELM327's request and response, adopted from [26].

9.1 Internal combustion engine vehicle

Table 8, lists the data logged for energy measurement purposes. Since fuel pumps are not available on-site, fuel consumption of internal combustion engine vehicle (Mazda CX7) is estimated based on OBD-II data. First, fuel flow rate was modeled as a function of available OBD-II signals and one data-driven parameter. The fuel estimation model was then validated using fuel volume and flow data available from a flow meter during a chassis dynamometer calibration test. Finally, the calibrated model was applied to OBD-II data from the test track to record fuel consumption.

Table 8. Basic OBD Data collected for energy usage estimation (Internal combustion engine vehicle).

Data Name	Data Type and Unit	Collection Method	Sampling Rate
Fuel System Status	Discrete (0 to 6)	OBD port	8 Hz max
Commanded Equivalence Ratio	Continuous	OBD port	8 Hz max
Mass Air-flow	Continuous (g/s)	OBD port	8 Hz max
Short Term Fuel Trim	Continuous (%)	OBD port	8 Hz max
Long Term Fuel Trim	Continuous (%)	OBD port	8 Hz max
Calculated Engine Load Value	Continuous (%)	OBD port	8 Hz max

Fuel injector flow rate, pulse width, or a similar quantity was not available on the test vehicle, so fuel rate was modeled using ECU-estimated mass airflow (MAF), commanded λ, and a derived MAF correction curve. As background, the air-fuel ratio of a conventional gasoline engine is typically near stoichiometric to promote stable combustion, high efficiency, and low emissions. However, a mildly rich λ of 0.85 to 0.91 can increase maximum torque. Even richer mixtures are sometimes used to limit exhaust gas temperatures, particularly in turbocharged applications. The test vehicle's OBD-II data includes the ECU-commanded air-fuel ratio in the form of $\lambda = m_{fs}/m_f$ where m_{fs} and m_f denote the stoichiometric and actual mass fuel flow, respectively. The fuel flow that the ECU commands is modeled as follows.

$$\dot{m}_f = \frac{\dot{m}_a}{AFR_s \lambda_c} \overline{E}_A(\dot{m}_a) \tag{17}$$

A stoichiometric air-fuel ratio $AFR_s = 14.1$ was used for the 10% ethanol pump fuel that is commonly available in the United States.

In Eqn. (17), E_A is a correction factor to the ECU-estimated mass airflow. λ is normally closed-loop controlled to stoichiometric using an exhaust oxygen sensor. Long-term and short-term correction factors called *trims* are applied to the fuel pulse width such that the desired λ is delivered. These trims are denoted *LTFT* and *STFT*, respectively. Errors in both airflow measurement and fuel system modeling contribute to these fuel trims. Assuming that fuel system model deviation results from a change in effective orifice size, Eqn. (18) assumes that the trim due to the fuel system is a constant e_F with respect to mass airflow.

$$E_A = 1 + \frac{LTFT + STFT}{100} - e_F \tag{18}$$

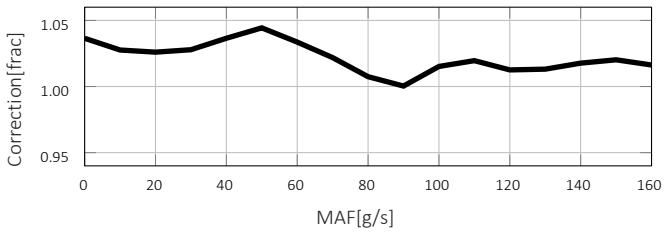

Figure 45: MAF correction factor and source fuel trim data.

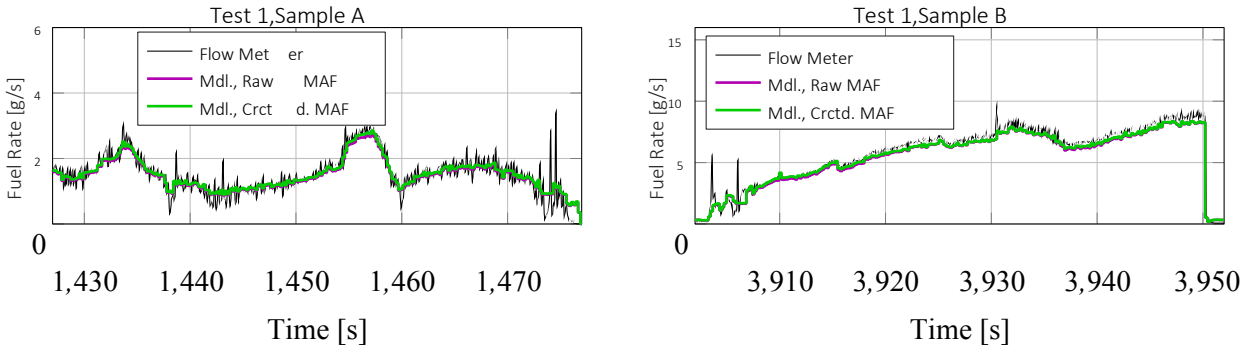

Figure 46: Comparison of OBD model-based fuel rate with and without MAF correction against fuel flow measurements.

Transient gas exchange dynamics and measurement delays generally affect fuel trims and their time-alignment with airflow estimates. Fuel trims are therefore scattered as a function of airflow, although trends

do emerge over large datasets. So, E_A is not used directly, but rather averaged into bins to calibrate E_A - where M is the number of samples in the bin.

$$\overline{E}_A(\dot{m}_{aj}) = \frac{1}{M}\sum_{j=1}^{M} E_A \dot{m}_{aj} \tag{19}$$

9.1.1 Calibration and Validation

Closed-loop data from track tests of various algorithms was combined into a calibration dataset for E_A. Figure 45 shows the resulting correction, which is within 5% for all m_a. The OBD-based fuel flow model was validated in two ways: dynamically by comparison against measurements from a volume flow meter, and cumulatively by comparison against a measured volume of fuel placed in the empty tank. This fuel was also weighed to ensure accurate density. Figure 47 shows the flow meter calibration experiment, with an AVL KMA Mobile flow meter connected between the fuel tank and the high pressure fuel pump of the engine [23]. The SoMat eDAQ system [25] was used with the SoMat Test Control Environment software to collect fuel data.

Three tests were performed, all of which began with an empty fuel tank before putting a certain amount of fuel in the tank, as shown in Figure 48. For each test, the vehicle was run on a chassis dynamometer until it ran out of fuel. Test 3, during which 3 US gallons of fuel was consumed, was used to calibrate e_F. Tests 1 and 2 were reserved for validation. Figure 46 demonstrates qualitative model performance in lower and higher power samples from Test 1.

Table 9 lists the model's accuracy in the three chassis dynamometer tests where total fuel volume was directly measured. Test 2's flow meter and volume-based cumulative fuel measurements differed by 8.0%, exceeding the differences observed in the other tests and indicating a possible ground truth measurement error in Test 2. Therefore, the proposed OBD-based technique was adopted by virtue of its close match to the validation data in test 1 and acceptable match to the instantaneous fuel flow measurement in Figure 46.

Table 9: OBD model accuracy in cumulative fuel consumption

Test No.	Meas. Fuel Vol. [L]	Est. Fuel Vol. [L]
1 (validation)	3.79	3.79
2 (validation)	9.46	8.90
3 (calibration)	11.36	11.38

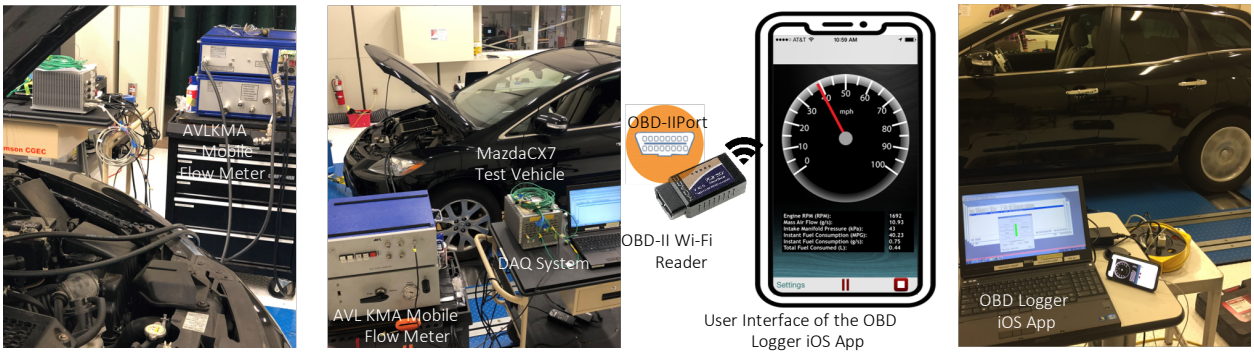

Figure 47: The AVL KMA Mobile fuel measurement system and the OBD-based fuel rate estimator connected to the combustion test vehicle

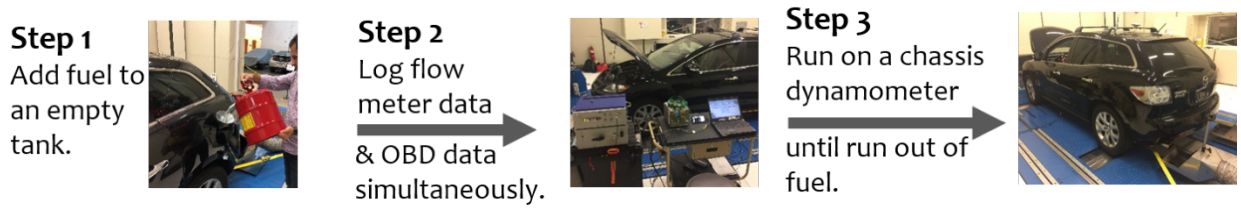

Figure 48: The steps to calibrate and evaluate our OBD-based fuel rate estimations.

9.2 Battery electric vehicle

Unlike the combustion engine vehicle, the specification of the electric vehicle's OBD data is not published by the vehicle manufacturer - mainly because the electric car manufacturers have not established a standard for messages exchanged from its CAN bus [28]. The existing smart phone applications for Nissan Leaf's OBD data collection, such as Leaf Spy [24], provide insufficient sample rates. Following the guidelines in [28] and verifying the results with that of Leaf Spy [24], OBD-based measurements were collected for the signed battery current, I, terminal voltage, V_T, state-of-charge, SOC, and capacity via the custom iOS app. Table 10, lists the data logged for energy measurement purposes.

Table 10. Basic OBD Data collected for energy usage estimation (Battery electric vehicle).

Data Name	Data Type and Unit	Collection Method	Sampling Rate
Battery Current	Continuous (A)	OBD port	4 Hz max
Battery Voltage	Continuous (V)	OBD port	4 Hz max
Battery State-of-Charge (SOC)	Continuous (%)	OBD port	4 Hz max
Battery Capacity	Continuous (Ah)	OBD port	4 Hz max

For the Li-ion battery of the Nissan Leaf, a lumped resistance R_s is considered. As shown in [27], the open-circuit voltage, V_{OC}, is assumed to have a linear relationship with SOC in the mid-range of SOC levels when considering fixed battery temperature (We assume that the ambient temperature is constant during our tests). So, the resulting linear model is fit to the collected OBD data to give an estimated value of $R_s = 0.1\Omega$. As the obtained resistive loss is negligible compared to the battery net energy, and each test consisted of similar ambient temperatures, R_s was assumed constant for all tests. Considering the resistive energy loss, the battery net energy is then obtained by integrating over the entire test interval.

$$E_{battery} = \int_{t_0}^{t_1} \left(V_T(t)\, I(t) + R_s I^2(t)\right) dt \tag{20}$$

$$\approx \sum_{k=1}^{M} \left(V_T(t_{k-1})I(t_{k-1}) + V_T(t_k)I(t_k) + R_s I^2(t_{k-1}) + R_s I^2(t_k)\right) \frac{\Delta t_k}{2} \tag{21}$$

10) Simulation and control timing (Milestones 3.1.1, 3.2.1)

Timing mechanisms are defined in the server layer for precisely controlling the simulation environment to run in real-time and broadcast updates on its status in regular intervals of 10hz, and are defined in the client layer for broadcasting the ego vehicle's status in regular intervals of 10hz - so that the vehicle can provide feedback to the simulation for surrounding virtual traffic to react to. Because multiple computers are involved, a Network Time Protocol (NTP) was introduced to synchronize the clocks and regularly measure

communication delay [29]. In this case, as shown in Figure 49, the client polls the server for its clock time, and makes an adjustment to its own clock by measuring a time-offset t', and round-trip delay Δt,

$$t' = \frac{(t_1 - t_0) - (t_2 - t_3)}{2} \tag{22a}$$

$$\Delta t = (t_3 - t_0) - (t_2 - t_1) \tag{22b}$$

where t_0, t_3 are the client's request and reception message timestamps, and t_1, t_2 are the server's reception and response message timestamps. Most recent round-trip delays are used by the client and server to interpolate positional data from the ego vehicle and its preceding vehicle.

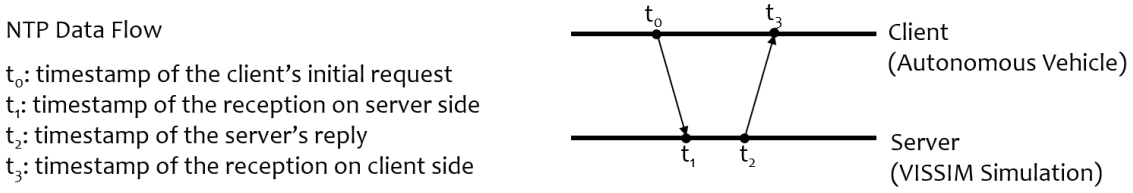

Figure 49: Network Time Protocol (NTP) implementation between the client and server layers of the VIL architecture.

10.1 Simulation data exchange

A client-server architecture was designated between the ego vehicle and simulation computer so that computational load could be split between multiple computers. Such a setup also has the advantage of allowing co-simulation of multiple clients at once - suitable for future experiments.

In this case, exchange of key data between simulation and the ego vehicle was defined using a Google Protocol Buffer (Protobuf) serialization to byte arrays and then broadcast through the User-Datagram Protocol (UDP) socket communication [30]. UDP was chosen because of its low-latency data exchange and is suitable in systems with lower chances of packet loss. Protocol buffers are a mechanism to serialize data. We specify the structure of the data in a protocol buffer message format [31] which can be used to transfer data between our instrumented vehicles and our simulation server regardless of their implementation language. As claimed by Google and as evaluated in [32], the Protocol Buffer leads to fast data transfer over the web comparing to eXtensible Markup Language or XML [33]. This is mainly because the Protocol Buffer uses binary format to serialize structured data.

The data exchanged between the physical vehicle and the simulation server lies in four categories with their data structure shown in Figure 50: 1) Subscription/Un-subscription Message: A physical vehicle subscribes to the simulation server at the beginning of VIL simulations, or unsubscribes to end the simulation, 2) V2Sim Message: A physical vehicle transmits its updates (x, y, v, θ) to the simulation server, 3) Sim2V Message: the simulation server transmits information of the simulated vehicles surrounding the physical vehicle, and 4) V2V Message: the simulated and physical vehicles exchange planned trajectories for connected vehicle guidance (MPC-C).

Each message is preceded with a predefined preamble after being serialized by Google Protocol Buffers. In order to reduce the bandwidth challenges imposed on the simulation side, we incorporate the vehicle-to-vehicle (V2V) messaging into the Sim2V and V2Sim messages. The resulting buffer is only a few hundred bytes in size. Please note that the preamble should not be serialized; otherwise, the receiver should decode the received packet by trying all possible message types which can impose a huge performance penalty.

Subscription/Unsubscription Message:

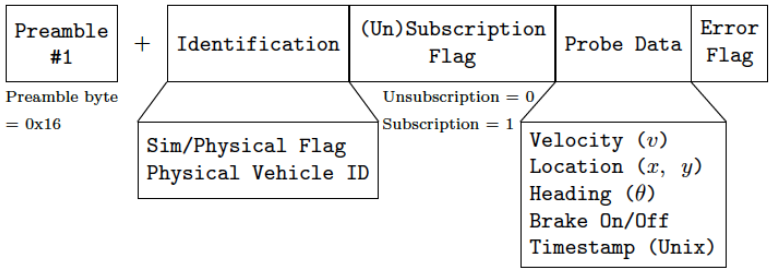

V2Sim Message:

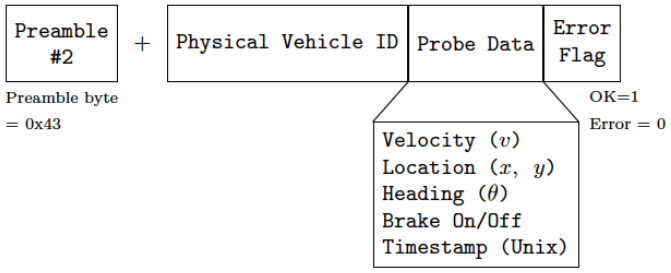

Sim2V Message:

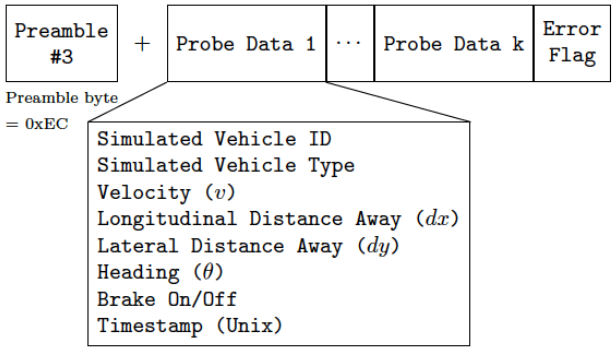

V2V Message:

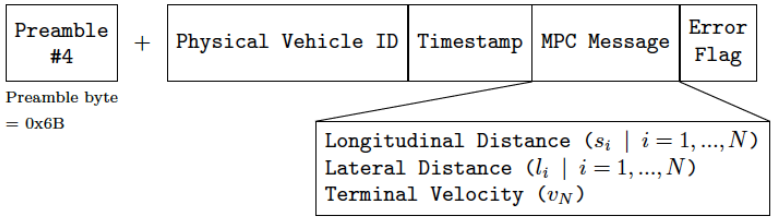

Figure 50: Four different message types implemented for the VIL test environment (Protocol buffer structured messages preceded with a preamble).

c. What opportunities for training and professional development has the project provided?

The project engaged two postdoctoral researchers, five Ph.D. Students, and one undergraduate student. Through working on the project and regular meeting with PIs they were trained on algorithm development, software development and simulation, and hardware implementation. Moreover, they got invaluable experience in team work, communication, and presentation and project management.

The following awards have been won by the students.

1. Longxiang Guo wins 2020 CECAS College Outstanding Graduate Researcher Award for his contribution to the team effort and in particular experimental testing of automated vehicles, 2020.
2. Best Paper Award, ASME Technical Committee on Automotive and Transportation Systems for "Predictively Coordinated Vehicle Acceleration and Lane Selection Using Mixed Integer Programming" by A. Dollar and A. Vahidi, 2019
3. Young Author Award, International Federation of Automatic Control for the paper "Chance Constrained Automated Vehicles in Hazardous Merging Traffic,", 2019
4. Advanced Vehicle Technologies Best Paper Award, ASME IDETC Conference, 2019
5. Austin Dollar selected as a recipient of a 2018-2019 STEM Chateaubriand Fellowship for eight-month research in France on topics related to team's collaboration, 2018.
6. The 2017 SAE Trevor O. Jones Outstanding Paper Award

d. How have the results been disseminated to communities of interest?

A number of papers have been published, presented at various conferences, and submitted for review and are listed in the publication section. Additionally, an overview of the project methods and results have been prepared in a presentation to be shared with a number of government, industry, and research partners. An on-site demonstration was scheduled for March 24, 2020 with confirmed participants from GM, Ford, BMW, Toyota, Cummins, Commsignia, PTV group, Allision Transmissions, ZF, Michelin, Southwest Research Institute, Argonne National Lab, and Oakridge National Lab. An executive summary of the project had been distributed which provided exposure for the project. Unfortunately, the demo had to be canceled in mid-March due to the shut-down imposed by the 2020 Pandemic.

Encouraged by the results and with support of two technical experts from General Motors, has been submitted to GM with the goal of continued experimental testing and extending some of the ideas developed in this project to the industry.

III. Products

a. Publications, conference papers, and presentations

- T. Ard, L. Guo, R. A. Dollar, A. Fayazi, N. Goulet, Y. Jia, B. Ayalew, and A. Vahidi. "Energy-Efficient Automated Car-Following: Vehicle-in-the-Loop Field Results." *Transportation Research Part C*, in review, 2020.

- L. Guo and Y. Jia. "Combine Heuristic AI based Control with Analytic Model Formed Control for Automated Vehicles." In Review, *IEEE Transactions on Vehicular Technology* (2020).

- T. Ard, R. A. Dollar, D. Karbowski, Y. Zhang, and A. Vahidi. "Evaluating the Impact of Automated Vehicles with Optimal Eco-Driving in High Fidelity Traffic Microsimulations." , *Transportation Research Part C*, **120**, 2020.

- G. G. M. Nawaz Ali, Beshah Ayalew, Ardalan Vahidi, and Md. Noor-A-Rahim, "Feedbackless Relaying for Enhancing Reliability of Connected Vehicles," *IEEE Transactions on Vehicular Technology*, **69**, 4621 – 4634, 2020

- G. G. M. Nawaz Ali, Beshah Ayalew, Ardalan Vahidi, and Md. Noor-A-Rahim, "Analysis of Reliabilities Under Different Path Loss Models in Urban/Sub-urban Vehicular Networks", to appear, *Proceedings of IEEE 90th Vehicular Technology Conference* (IEEE VTC-Fall'19), Honolulu, HI, 2019.

- Goulet, N. and Ayalew, B. "Coordinated Model Predictive Control on Multi-Lane Roads". In *Proceedings of the ASME 2019 International Design Engineering Technical Conferences & Computers and Information in Engineering Conference* (IDETC 2019). August 18-21, 2019. Anaheim, CA, USA.

-D. Yoon and B. Ayalew (2019) "D. Yoon and B. Ayalew (2019) "Hierarchical Vehicular Social Force Control for Human-like Autonomous Driving," *Proceedings of the American Control Conference*, July 10-12, Philadelphia, PA

- R. Dollar and A Vahidi, "Automated Driving with Variational Optimal Control and Mixed Integer Programming," in review, *IEEE Transactions on Control Systems Technology*, 2019.

- R. Dollar and A. Vahidi, "Chance Constrained Automated Vehicles in Hazardous Merging Traffic," in *Proceedings of IFAC Conference on Advances in Automotive Control,* Orleans, France, 2019. **Won IFAC's Best Young Author Award.**

- R. Austin Dollar, and Ardalan Vahidi. "Predictively Coordinated Vehicle Acceleration and Lane Selection Using Mixed Integer Programming." in *Proceedings of the ASME DSCC*, 2018. **Won Automotive and Transportation Systems Technical Committee Best Paper Award.**

- R. Austin Dollar, and Ardalan Vahidi. "Efficient and Collision-Free Anticipative Cruise Control in Randomly Mixed Strings." *IEEE Transactions on Intelligent Vehicles*, 3, 439-452, 2018.

- R. Austin Dollar, and Ardalan Vahidi. "Quantifying the impact of limited information and control robustness on connected automated platoons." In *Proceedings son IEEE Conference on Intelligent Transportation Systems* (ITSC), 2017.

- N. Goulet and B. Ayalew. "Impacts of Distributed Speed Harmonization and Optimal Maneuver Planning on Multi-Lane Roads." To Appear, 2020 Conference on Control Technologies and Applications.

- R. A. Dollar, A. Sciarretta, and A. Vahidi. “Multi-Agent Control of Lane-Switching Automated Vehicles for Energy Efficiency.” Presented, American Control Conference, 2020.

- R. A. Dollar, A. Sciarretta, and A. Vahidi. “Information and Collaboration Levels in Vehicular Strings: A Comparative Study.” Presented, IFAC World Congress, 2020.

- N. Goulet and B. Ayalew. “Distributed Maneuver Planning with Connected and Automated Vehicles for Boosting Traffic Efficiency.” Submitted and in review, IEEE Transactions on Intelligent Transportation Systems.

Presentations:

- A. Vahidi, "Energy and Flow Effects of Optimal Automated Driving in Mixed Traffic", online, New York University, Abu Dhabi, November 8, 2020.

- A. Vahidi, "Vehicle-in-Loop Experiments of Optimal Automated Driving in Mixed Traffic" PTV Group North America, Virtual Webinar, October 15, 2020.

- A. Vahidi, "Efficient Driving Leveraging Cellular Connectivity," virtual, Qualcomm, San Diego, CA, September 28, 2020.

- A. Vahidi, "Anticipative Guidance of Connected and Autonomous Cars for Energy Efficiency," Workshop on Emerging Control of Vehicular Traffic for Improving Sustainability and Energy Efficiency, Society of Instrument and Control Engineers (SICE) Annual Conference, Chiang Mai, Thailand, September 23, 2020.

- A. Vahidi, "Eco Driving with Connected and Automated Vehicles", Department of Mechanical and Industrial Engineering, University of Ilinois at Chicago, January 28, 2020.

- A. Vahidi, "Eco Driving with Connected and Automated Vehicles", Workshop on Connected and Automated Vehicles for Energy Efficiency and Environment Impact, IFP Energies Nouvelles, Rueil-Malmaison, France, September 30, 2019.

- A. Vahidi, "Anticipative Guidance of Connected and Autonomous Cars for Energy Efficiency" IDETC-CIE, Anaheim, CA, August 2019.

- A. Vahidi, "Opportunities for Efficient Driving with CAVs and Their Network-wide Impact" NSF Workshop on Control for Networked Transportation Systems, Philadelphia, PA, July 8-9, 2019.

- A.Vahidi, "Eco-driving with Connected and Automated Vehicles: Algorithms and Experiments" 3rd IAVSD Workshop on Dynamics of Road Vehicles: Connected and Automated Vehicles, University of Michigan, Ann Arbor, April 28, 2019.

- A. Vahidi, "Eco-Driving with Connected and Automated Vehicles", ASME DSCC, Workshop on Connected and Automated Vehicles, Atlanta, GA, September 30, 2018.

- A. Vahidi, "Anticipative Guidance of Connected and Autonomous Cars for Energy Efficiency," Research and Innovation Center, Ford Motor Company, May 17, 2018.

- Y. Jia, "Human Intervention Detection on a Retrofit Steering Actuation System in Autonomous Vehicles," Keynote in Connect2Car at SAE World Congress Experience (WCX), Detroit, MI, April 12, 2018.

- A. Vahidi, "Optimal Coordination of Connected and Autonomous Cars in Smart Cities", University of California, Berkeley, November 3, 2017 (please see [7]).

- A. Vahidi, "Optimal Coordination of Connected and Autonomous Cars in Smart Cities", New York University, Abu Dhabi, November 19, 2017.

Relevant Indirect Products:

- X. Wang, L. Guo and Y. Jia, "Online Sensing of Human Steering Intervention Torque for Autonomous Driving Actuation Systems," *IEEE Sensors Journal*, vol. 18, no. 8, pp. 3444-3453, 2018

- X. Wang, L. Guo and Y. Jia, "Human Intervention Detection on a Retrofit Steering Actuation System in Autonomous Vehicles," SAE World Congress, 2018. **Won SAE Trevor O. Jones Outstanding Paper Award.**

- A. Vahidi and A. Sciarretta, "Energy Saving Potentials of Connected and Automated Vehicles," *Transportation Research Part C*, **95**, 822-843, 2018.

- J. Han, A. Vahidi and A. Sciarretta, "Fundamentals of Energy Efficient Driving for Combustion Engine and Electric Vehicles: An Optimal Control Perspective," accepted, Automatica, 2018.

- Q. Wang, B. Ayalew and T. Weiskircher "Predictive Maneuver Planning for an Autonomous Vehicle in Public Highway Traffic," in review, IEEE Transactions on Intelligent Transportation Systems (2018).

- Q. Wang and B. Ayalew (2017), "Probabilistic Constraint Tightening for Predictive Guidance of an Autonomous Vehicle in Multi-Vehicle Traffic", in review, IEEE Transactions in Robotics.

- A. Hunde and B. Ayalew (2018), "Automated Multi-Target Tracking in Public Traffic in the Presence of Data Association Uncertainties" Accepted for publication, Proceedings of the American Control Conference, June 27-29, Milwaukee, WI.

- D. Gundana, R. A. Dollar and A. Vahidi, "To Merge Early or Late: Analysis of Traffic Flow and Energy Impact in a Reduced Lane Scenario." To be presented, Intelligent Transportation Systems (ITSC), 2018 IEEE 21st International Conference on, 2018.

-A. Hunde, B. Ayalew and Q. Wang (2019) "Automated Multi-Object Tracking for Autonomous Vehicle Control in Dynamically Changing Traffic," *Proceedings of the American Control Conference*, July 10-12, Philadelphia, PA (in review).

b. Websites or other Internet sites

Video of autonomous Nissan Leaf: https://www.youtube.com/watch?v=ekcnKJGLm7w

Video of autonomous Mazda CX-7: https://www.youtube.com/watch?v=LMsJKHJ72R0

c. Technologies or techniques

ITIC received valuable input to improve their smart mobility testbed through V2X capabilities which allow both car manufacturers as well as suppliers to test AV scenarios in mixed reality configurations emulating real world traffic conditions. That capabilities can be used in the future to classify and potentially certify smart mobility testbed through consortiums such as SAE/IEEE-supported International Alliance for Mobility Testing and Standardization (IAMTS).

d. Inventions, patent applications, and/or licenses

Nothing to report in this quarterly report.

e. Other products

1. Automotive News, "'Ghost' AV research may put the brakes on stop-and-go traffic", June 18, 2020.
2. ASEE's First Bell, "Clemson Researchers Develop Technology To Help Autonomous-Driving Vehicles Save Energy," June 18, 2020
3. Clemson News, "'Ghost' vehicle research shows energy savings in self-driving cars", June 17, 2020.
4. Government Report by NSTC and US DOT, "Ensuring American Leadership in Automated Vehicle Technologies - Automated Vehicles 4.0," January 2020.
5. Upstate Business Journal, "How automotive testing in Greenville could impact tomorrow's roadways" (September 2019)
6. Upstate Business Journal, "How Clemson researchers plan to boost energy efficiency with connected, automated vehicle technology" (August 2017)
7. Greenville News, "Clemson awarded $1.16M to research use of connected, automated vehicle technology to boost energy efficiency" (July 2017)

IV. Participants and Collaborating Organizations

a. What individuals have worked on the project?

1)	Name:	Prof. Ardalan Vahidi
	Project Role:	PI (Clemson University)
	Researcher Identifier:	NA
	Total number of months:	30
	Contribution to Project:	Prof. Vahidi is the lead investigator and has been responsible for the administration of the research grant. He has also been directly supervising his graduate students.
	State, and country of residence:	SC, USA
2)	Name:	Dr. Yunyi Jia
	Project Role:	Co-PI
	Researcher Identifier:	NA
	Total number of months:	30
	Contribution to Project:	Dr. Jia has been leading a team responsible for vehicle instrumentation and design of the autonomous driving controls.
	State, and country of residence:	SC, USA
3)	Name:	Dr. Beshah Ayalew
	Project Role:	Co-PI (Clemson University)
	Researcher Identifier:	https://orcid.org/0000-0002-3759-3271
	Total number of months:	30
	Contribution to Project:	Dr. Ayalew has been working on developing the lane selection scheme as part of our predictive autonomous vehicle guidance scheme.
	State, and country of residence:	SC, USA
4)	Name:	Mr. Dominik Karbowski
	Project Role:	Co-PI (Argonne National Laboratory-ANL)
	Researcher Identifier:	NA
	Total number of months:	30
	Contribution to Project:	Mr. Karbowski has been working on estimating energy efficiency using ANL's detailed powertrain simulation tool Autonomie.
	State, and country of residence:	IL, USA

5)	Name:	Prof. Joachim G. Taiber
	Project Role:	Sub-contractor (International Transportation Innovation Center-ITIC)
	Researcher Identifier:	NA
	Total number of months:	30
	Contribution to Project:	Prof. Taiber, as the CTO of ITIC, has been managing the communication network design and implementation and the interfaces to the IT backend at the ITIC testbed facility.
	State, and country of residence:	SC, USA

6)	Name:	Dr. Ali Reza Fayazi
	Project Role:	Post-doctoral fellow (Clemson University)
	Researcher Identifier:	https://orcid.org/0000-0002-8560-2873
	Total number of months:	30
	Contribution to Project:	Dr. Fayazi has been monitoring the project progress, and setting up project management tools. He has also been working on goals related to the vehicle-in-the-loop simulation environment.
	State, and country of residence:	SC, USA

7)	Name:	Dr. G. G. Md. Nawaz Ali
	Project Role:	Post-doctoral fellow (Clemson University)
	Researcher Identifier:	https://orcid.org/0000-0001-5861-0475
	Total number of months:	21
	Contribution to Project:	Dr. Nawaz worked on vehicular simulation and V2X communication with VISSIM, MATLAB and ns-3 environments.
	State, and country of residence:	SC, USA

8)	Name:	R. Austin Dollar
	Project Role:	PhD Student (Clemson University)
	Researcher Identifier:	NA
	Total number of months:	30
	Contribution to Project:	Mr. Dollar has been developing the anticipative vehicle guidance algorithms. He is working under supervision of Prof. Vahidi.
	State, and country of residence:	SC, USA

9)	Name:	Tyler Ard
	Project Role:	PhD Student (Clemson University)
	Researcher Identifier:	NA
	Total number of months:	30
	Contribution to Project:	Mr. Ard has been working on the goals related to the traffic microsimulation and vehicle-in-the-loop experimental platforms. He is working under supervision of Prof. Vahidi.
	State, and country of residence:	SC, USA

10)	Name:	Longxiang Guo
	Project Role:	PhD Student (Clemson University)
	Researcher Identifier:	NA
	Total number of months:	29
	Contribution to Project:	Mr. Guo is working on the goals related to vehicle instrumentation and improving the design of the autonomous driving controls. He is working under supervision of Dr. Jia.
	State, and country of residence:	SC, USA
11)	Name:	Nathan Goulet
	Project Role:	PhD Student (Clemson University)
	Researcher Identifier:	NA
	Total number of months:	28
	Contribution to Project:	Mr. Goulet is working on the goals related to the anticipative lane change maneuver algorithm. He is working under supervision of Dr. Ayalew.
	State, and country of residence:	SC, USA

Figure 51: The project team during the 2018 annual visit by DOE program managers.

b. Has there been a change in the active other support of the PD/Pl(s) or senior/key personnel since the last reporting period?

No.

c. What other organizations have been involved as partners?

Clemson University worked with the following organizations as partners on this project:

- Argonne National Laboratory to integrate the vehicle guidance algorithms with Autonomie, Argonne's detailed vehicle energy utilization simulation software.
- PTV Group: to incorporate the proposed algorithms in PTV Group's traffic micro-simulation tool (VISSIM).
- International Transportation Innovation Center (ITIC): to provide the experimentation platform for evaluating the proposed technical approach with novel co-simulations of traffic and physical connected and automated vehicles on a cyber-physical test track.

d. Have other collaborators or contacts been involved?

Collaborative guidance research was co-supervised by P.I. Ardalan Vahidi and Dr. Antonio Sciarretta of IFP Energies nouvelles.

V. Impact

What is the impact of the project? How has it contributed?

The project has contributed to the state of art of energy efficient driving by developing advanced vehicle guidance algorithms that save energy while preserving safety and traffic compactness. If the project's proposed and experimentally verified methods are adopted in new vehicles and in particular automated vehicles, there can be significant reduction in energy consumption and greenhouse emissions. These savings can materialize immediately upon implementation, mostly via software, and with minimal additional hardware investments. More details are described below.

a. What was the impact on the development of the principal discipline(s) of the project?

The algorithms developed under this project are expected to be adopted by other researchers and practitioners in the field of energy efficient driving and automated driving. We have taken the algorithms beyond academic research by showcasing their positive energy impact in field tests without compromising safety, traffic flow, and travel time. The methods have the potential for real-time implementation. And they can be deployed in mixed traffic where human-driven vehicles are present. The DOE funding enabled us to perfect the algorithms beyond what is normally shown in academic papers and advance the field of eco-driving.

As stated elsewhere, the vehicle-in-the-loop testing technology can potentially impact vehicle certification and testing and in particular testing of automated vehicles.

b. What was the impact on other disciplines?

Our algorithms and testing algorithms are likely to make an impact on automated vehicle development and certification.

c. What was the impact on the development of human resources?

Four PhD students completed major parts of their dissertation research based on their contributions to this project. The project has been an excellent scientific, technical, and project management opportunity for these students. The students have received considerable visibility via conference presentation and in the news media. When they join the industry or academic work force, they carry the valuable experience of having worked on a sizable team project with ambitious outcomes that they have achieved.

Two postdoctoral fellows worked on this project. One has joined academia as an assistant professor and the other has joined a Silicon Valley startup working on automated driving and ride sharing.

One undergraduate student (and a minority) participated in early stages of the project and published a peer-reviewed conference paper which is unusual for an undergraduate student. He is now a Ph.D. student at Cornell University.

The project has also provided the PIs the opportunity to advance their knowledge in the novel field of automated driving; this knowledge can be imparted in their classes to wider students and contribute to advancement of their future research.

d. What was the impact on teaching and educational experiences?

The PI has recently co-authored and published a book on energy efficient driving of connected and automated vehicles with international reach and includes some of the results of this project. The findings of the project provide excellent and sensible motivating examples for our undergraduate and graduate classes. The students relate to cars, get excited by automation, and care about energy impact. Showing even a video of the test track experiments along with basic underlying technical concepts, goes a long way in our classes to get the students excited and motivated to pursue careers or graduate education in line with the goals of this DOE VTO project.

The findings of the project have been presented in several invited talks nationally and internationally and as a result many experts in the field have seen different stages of the project findings via these talks. Examples are workshops on connected and automated vehicles in Atlanta (2018), The University of Michigan (2019) IFP, France (2019), and an NSF sponsored workshop on connected transportation systems held in 2019 in Philadelphia.

e. What was the impact on physical, institutional, and information resources that form infrastructure?

Testing in this project consisted of one electric vehicle (Nissan Leaf) and one gasoline engine vehicle (Mazda CX-7). These vehicles were not equipped with automated driving capabilities from the manufacturer, so they were modified to execute the commands from the high-level controller autonomously. The modifications include adding necessary sensors, actuators, and designing control algorithms. These vehicles are now available for educational and research purposes. The vehicles were tested at ITIC test track in Greenville, South Carolina. A Vehicle-in-the-loop platform has been built that allows testing these vehicles while surrounded by virtual vehicles reducing or eliminating collision risk. This mostly-software-based VIL platform provides many future possibilities for testing automated vehicles. Moreover DSRC equipment has been deployed and programmed for V2V communication that extends testing capabilities at ITIC.

f. What was the impact on technology transfer?

The Vehicle-In-Loop testing platform that we have developed has a clear potential for technology transfer as it could reduce the cost and risk of connected and automated vehilces testing and certification. Several companies have expressed interest in the concept. We have submitted a research proposal to General Motors that proposed to utilize VIL experiments. The PI is working with Cummins on another DOE funded project (on truck platooning) that may use our VIL architecture. Researcher at Argonne National Lab are also interested in utilizing our VIL platform. The test track operator, ITIC, received valuable input to improve their smart mobility testbed through V2X capabilities which allow both car manufacturers as well as suppliers to test AV scenarios in mixed reality configurations emulating real world traffic conditions. That capabilities can be used in the future to classify and potentially certify smart mobility testbed through consortiums such as SAE/IEEE-supported International Alliance for Mobility Testing and Standardization (IAMTS).

Our published eco-driving algorithms can be prime candidates for adoption by industry as they have been successful in proof-of-concept experimental demos.

g. What was the impact on society beyond science and technology?

Our research advances the state-of-art in self-driving cars and also connected vehicle technologies. Our proposed algorithms, if implemented, can reduce energy consumption and green house emissions significantly (8-23% if widely deployed) which has direct positive environmental and societal impact.

h. What percentage of the award's budget was spent in foreign country(ies)?

Only one conference paper was presented in Europe. The expenditure was only conference registration and lodging. The student presenter was already on a fellowship residency in Europe so there were no foreign travel expenses.

VI. Changes

The last task is not complete due to 2020 pandemic shutdowns that prevented us from conducting test track experiments after March 7, 2020. All the low-level control functions are implemented on the car and were tested on the test track before March 7. The high-level algorithms are all in mature shape and tested in microsimulations. Only test track verification of lane change remains and is expected to be done over a

few days once we are able to test. We have completed all other test track testing on car following scenarios as presented in this report. We plan to complete 2 days of testing once we can go back to the test track after project close-out so we can write the paper we intend to write on the topic.

VII. Special Reporting Requirements

NA.

VIII. Budgetary Information

The quantitative budget information is submitted separately in the Federal Financial Report.

IX. Project Outcomes

- Novel car-following and lane selection algorithms that can save energy in presence of human driven vehicles and without compromising road capacity and travel time. Proven performance in large scale microsimulations, high fidelity fuel economy evaluations, and road experiments with gasoline and electric vehicles.
- Demonstrated capabilities of our proposed Vehicle-In-the-Loop (VIL) experimental platform that enables testing CAVs in challenging traffic scenarios while eliminating risk of collision or injury. Full integration of VIL with a commercial traffic microsimulation software, with robust software and V2V communication architecture. Potential for wider use and impact in automated vehicle industry.
- Showcased the real-time implementation of sophisticated optimization-based control algorithms on experimental vehicles driving at highway speeds that limits the reaction times.
- Perfected sensing, localization, and low-level pedal and steering control algorithms for precise execution of eco-driving maneuvers. Approach can be extended to other automated vehicle development and research activities.
- Characterized realistic hurdles such as influence of packet drops and communication delays via simulation and in experiments.

X. References

[1] R. A. Dollar, A. Sciarretta, and A. Vahidi. “Multi-Agent Control of Lane-Switching Automated Vehicles for Energy Efficiency.” Accepted, American Control Conference, 2020.

[2] World Forum for Harmonization of Vehicle Regulations (2015). Proposal for amendments to global technical regulation no. 15 on worldwide harmonized light vehicles test procedure. Technical Report ECE/TRANS/WP.29/GRPE/2016/3, United Nations, Geneva.

[3] R. A. Dollar, A. Sciarretta, and A. Vahidi. “Information and Collaboration Levels in Vehicular Strings: A Comparative Study.” In review, IFAC World Congress, 2020.

[4] N. Goulet and B. Ayalew. "Impacts of Distributed Speed Harmonization and Optimal Maneuver Planning on Multi-Lane Roads." Submitted and in review, 2020 Conference on Control Technologies and Applications.

[5] Islam, E., A. Moawad, N. Kim, and A. Rousseau, An Extensive Study on Vehicle Sizing, Energy Consumption and Cost of Advance Vehicle Technologies, Report No. ANL/ESD-17/17, Argonne National Laboratory, Lemont, Ill., Oct 2018.

[6] R. A. Dollar, and A. Vahidi. "Efficient and collision-free anticipative cruise control in randomly mixed strings." *IEEE Transactions on Intelligent Vehicles* 3, no. 4 (2018): 439-452.

[7] T. Ard, R. A. Dollar, A. Vahidi, Y. Zhang, and D. Karbowski. "Microsimulation of Energy and Flow Effects from Optimal Automated Driving in Mixed Traffic." *arXiv preprint arXiv:1911.06818* (2019).

[8] R. A. Dollar and A. Vahidi. "Automated Vehicles in Hazardous Merging Traffic: A Chance-Constrained Approach." *IFAC-PapersOnLine* 52, no. 5 (2019): 218-223.

[9] Gurobi Optimization, Incorporate. "Gurobi optimizer reference manual." *URL http://www. gurobi. com* (2018).

[10] R. A. Dollar and A. Vahidi. "Predictively coordinated vehicle acceleration and lane selection using mixed integer programming." In *Dynamic Systems and Control Conference*, vol. 51890, p. V001T09A006. American Society of Mechanical Engineers, 2018.

[11] A. Sciarretta and A. Vahidi. *Energy-Efficient Driving of Road Vehicles*. Springer International Publishing, 2020.

[12] R. A. Dollar and A. Vahidi. “Automated Driving with Variational Optimal Control and Mixed Integer Programming.” *IEEE Transactions on Control Systems Technology*, in review, 2020.

[13] M. Treiber, A. Hennecke, and D. Helbing. "Congested traffic states in empirical observations and microscopic simulations." *Physical review E* 62, no. 2 (2000): 1805.

[14] T. Ard, L. Guo, R. A. Dollar, A. Fayazi, N. Goulet, Y. Jia, B. Ayalew, and A. Vahidi. “Energy-Efficient Automated Car-Following: Vehicle-in-the-Loop Field Results.” *Journal of Field Robotics*, in review, 2020.

[15] Goulet, N. and Ayalew, B. “Coordinated Model Predictive Control on Multi-Lane Roads”. In Proceedings of the ASME 2019 International Design Engineering Technical Conferences & Computers and Information in Engineering Conference (IDETC 2019). August 18-21, 2019. Anaheim, CA, USA.

[16] N. Goulet and B. Ayalew. “Distributed Maneuver Planning with Connected and Automated Vehicles for Boosting Traffic Efficiency.” Submitted and in review, IEEE Transactions on Intelligent Transportation Systems.

[17] T. Weiskircher, Q. Wang, and B. Ayalew (2017) “A Predictive Guidance and Control Framework for (Semi-) Autonomous Vehicles in Public Traffic”, IEEE Transactions in Control Systems Technology, Vol. PP, Issue: 99, PP 1-13

[18] PTV Group, “PTV Vissim 10 User Manual,” 2018.

[19] Halbach, Shane, Phillip Sharer, Sylvain Pagerit, Aymeric P. Rousseau, and Charles Folkerts. Model architecture, methods, and interfaces for efficient math-based design and simulation of automotive control systems. No. 2010-01-0241. SAE Technical Paper, 2010.

[20] Islam, E., A. Moawad, N. Kim, and A. Rousseau, An Extensive Study on Vehicle Sizing, Energy Consumption and Cost of Advance Vehicle Technologies, Report No. ANL/ESD-17/17, Argonne National Laboratory, Lemont, Ill., Oct 2018.

[21] Fayazi, S. A. and Vahidi, A. (2017). Vehicle-in-the-loop (VIL) verification of a smart city intersection control scheme for autonomous vehicles. In 2017 IEEE Conference on Control Technology and Applications (CCTA), pages 1575–1580. IEEE.
[22] Fayazi, S. A., Vahidi, A., and Luckow, A. (2019). A vehicle-in-the-loop (VIL) verification of an all-autonomous intersection control scheme. Transportation Research Part C: Emerging Technologies, 107:193 – 210.
[23] Online: AVL KMA mobile fuel consumption measurement system. https://www.avl.com/-/avl-kma-mobile
[24] Online: Leafspy pro. https://apps.apple.com/us/app/leafspy-pro/id967376861
[25] Online: Somat eDAQ and Somat eDAQXR data acquisition systems. https://www.hbm.com/en/7775/edaqxr-edaq-mobile-rugged-data-acquisition-systems/
[26] ELM Electronics (2012). ELM327, OBD to RS232 interpreter. https://www.elmelectronics.com/%20wp-content/uploads/2017/01/ELM327DS.pdf
[27] Parvini, Y., Vahidi, A., and Fayazi, S. A. (2017). Heuristic versus optimal charging of supercapacitors, lithium-ion, and lead-acid batteries: An efficiency point of view. IEEE Transactions on Control Systems Technology, 26(1):167–180.
[28] Tseng, C.-M., Zhou, W., Al Hashmi, M., Chau, C.-K., Song, S. G., and Wilhelm, E. (2016). Data extraction from electric vehicles through OBD and application of carbon footprint evaluation. In Proceedings of the Workshop on Electric Vehicle Systems, Data, and Applications, pages 1–6.
[29] Mills, D. L. (2010). Computer Network Time Synchronization: The Network Time Protocol on Earth and in Space, Second Edition. CRC Press, Inc., USA, 2nd edition.
[30] J. Postel, User datagram protocol, STD 6, RFC 768. URL http://www.ietf.org/rfc/rfc0768
[31] G. P. Buffer, https://developers.google.com/protocol-buffers/docs/overview
[32] G. Kaur, M. M. Fuad, An evaluation of protocol buffer, in: Proceedings of the IEEE SoutheastCon 2010, Charlotte-Concord, NC, USA, 2010, pp. 459-462.
[33] T. Bray, J. Paoli, C. M. Sperberg-McQueen, E. Maler, F. Yergeau, Extensible markup language (xml) 1.0, W3C Recommendation. URL http://www.w3.org/TR/REC-xml/